# Geometry-Assisted Localization Algorithms for Wireless Networks

Po-Hsuan Tseng, *Member*, *IEEE*, and Kai-Ten Feng, *Member*, *IEEE*

**Abstract**—Linear estimators have been extensively utilized for wireless location estimation for their simplicity and closed form property. In the paper, the class of linear estimator by introducing an additional variable, e.g., the well-adopted linear least squares (LLS) estimator, is discussed. There exists information loss from the linearization of location estimator to the nonlinear location estimation, which prevents the linear estimator from approaching the Cramér-Rao lower bound (CRLB). The linearized location estimation problem-based CRLB (L-CRLB) is derived in this paper to provide a portrayal that can fully characterize the behavior for this type of linearized location estimator. The relationships between the proposed L-CRLB and the conventional CRLB are obtained and theoretically proven in this paper. As suggested by the L-CRLB, higher estimation accuracy can be achieved if the mobile station (MS) is located inside the convex hull of the base stations (BSs) compared to the case that the MS is situated outside of the geometric layout. This result motivates the proposal of geometry-assisted localization (GAL) algorithm in order to consider the geometric effect associated with the linearization loss. Based on the initial estimation, the GAL algorithm fictitiously moves the BSs based on the L-CRLB criteria. Two different implementations, including the GAL with two-step least squares estimator (GAL-TSLS) and the GAL with Kalman filter (GAL-KF), are proposed to consider the situations with and without the adoption of MS's historical estimation. Simulation results show that the GAL-KF scheme can compensate the linearization loss and improve the performance of conventional location estimators.

**Index Terms**—Linear least squares (LLS) estimator, location estimation, Cramér-Rao lower bound (CRLB), two-step least squares estimator, Kalman filter

## 1 Introduction

Wireless location technologies [1], [2], [3], which are designated to estimate the position of a mobile station (MS), have drawn a lot of attention over the past few decades. The location estimation schemes locate the position of an MS based on the measured radio signals from its neighborhood base stations (BSs). It is recognized that the distance measurements associated with the wireless location estimation schemes are inherently nonlinear. The uncertainties induced by the measurement noises make it more difficult to acquire the MS's estimated position with tolerable precision. A number of wireless positioning methods have been widely studied with various types of signal measurements, including time-of-arrival (TOA), time difference-of-arrival (TDOA), and the received signal strength (RSS). Since the RSS measurements can be highly inaccurate because of the shadowing effect in practice, the distance-based TOA measurements will be considered in this work.

There are several representative techniques which are widely used in practical localization systems to deal with the location estimation problem (LEP), such as the Taylor series expansion-based (TSE) [4] method and the linear least squares (LLS) [5] method. The TSE method approximates the localization problem by taking the first two orders of Taylor expansion on the measurement inputs. Initial MS's position estimate and the iterative processes are required to obtain a location estimate from the linearized system based on the TSE scheme. The major drawback of the TSE method is that it may suffer from the convergence problem due to an incorrect initial guess of the MS's position. On the other hand, the original nonlinear estimation problem can be transformed into a linear relationship for the computation of MS's position by introducing an additional variable. This type of linearized methods deal with the linearized location estimation problem (L-LEP) and will be the major discussion in the paper. In general, the LLS is one of the popular techniques to solve the L-LEP in practical localization systems, e.g., the Cricket system [6], and has been continuously investigated from research perspectives [7], [8], [9], [10], [11]. Moreover, the closed form characteristic of LLS estimator is suitable for real-time implementation due to its computational efficiency.

The first objective of this paper is to formulate the theoretic lower bound for the geometric analysis of the L-LEP. Note that the Cramér-Rao lower bound (CRLB) serves as a benchmark of the non-Bayesian estimator. The CRLB for the conventional LEP is derived in [12], [13], and [14]. Since the LEP is inherently nonlinear, the original LEP is often transformed into an L-LEP by introducing an additional variable to transfer the nonlinear equation into a linear equation for the computation of MS's position. This transformation leads to a different parametrization and the geometric analysis of the L-LEP has not been fully addressed in previous research work. The work presented

- *P.-H. Tseng is with the Department of Electronic Engineering, National Taipei University of Technology, Taipei, Taiwan. E-mail: phtseng@ntut.edu.tw.*
- *K.-T. Feng is with the Department of Electrical and Computer Engineering, National Chiao Tung University, Hsinchu, Taiwan. E-mail: ktfeng@mail.nctu.edu.tw.*

*Manuscript received 22 Apr. 2011; revised 15 Nov. 2011; accepted 14 Feb. 2012; published online 7 Mar. 2012.*
*For information on obtaining reprints of this article, please send e-mail to: tmc@computer.org, and reference IEEECS Log Number TMC-2011-04-0210. Digital Object Identifier no. 10.1109/TMC.2012.61.*

in [15] provided a theoretic lower bound of L-LEP based on the maximum likelihood manner, which is equivalent to the CRLB under zero mean and independent Gaussian noises. In this paper, the performance analysis of L-LEP is conducted based on the theory of CRLB. The theoretical lower bound of the L-LEP is derived as the L-LEP-based CRLB (L-CRLB). Note that the main advantage of the derivation based on CRLB comparing to [15] is that the geometric properties can be captured from the formulation of L-CRLB. The closed form formulation of the Fisher information matrix (FIM) for the derived L-CRLB provides a comparison between the L-LEP and the conventional LEP. Since an additional variable other than the MS's position is required to be estimated for the L-LEP, it can be proved that the value of L-CRLB is greater than or equal to the conventional CRLB. The geometric layout between the MS and the BSs for the L-CRLB to be equivalent to the CRLB is also derived. By comparing the difference between the CRLB and the L-CRLB, it can be inferred from the proposed L-CRLB that better performance can be obtained if the MS is located inside the geometry constrained by the BSs; while inferior performance is acquired if the MS is outside of the geometric layout. Based on the observation, the geometry-assisted localization (GAL) algorithm is proposed.

In this paper, the GAL scheme is proposed to enhance the estimation precision by incorporating the geometric information within the conventional two-step least squares (LS) algorithm [9]. Note that the LLS method is one of the methods to solve the L-LEP; while the two-step LS is an performance enhancing estimator based on the LLS method. Since the linearization loss exists in the first step of the two-step LS estimator, the properties derived for the L-LEP can be utilized to describe the geometric effect of the two-step LS estimator. Based on an initial estimate of the MS's location, the GAL algorithm is proposed to fictitiously rotate (i.e., not to physically relocate) different BSs locations according to the L-CRLB criterion in order to achieve enhanced MSs location estimate. Reasonable location estimation can be acquired by adopting the GAL algorithm, especially feasible for the cases with poor geometric circumstances of the L-LEP, e.g., if the MS is located outside of the geometric layout confined by the BSs. Two different types of implementations are proposed for the GAL scheme, including the GAL with two-step LS estimator (GAL-TSLS) and the GAL with Kalman filter (GAL-KF) schemes. The GAL-TSLS can directly provide enhanced MS's location estimate compared to the conventional two-step LS method, which will be validated in the simulation results. The GAL-KF approach further uses the Kalman filter to provide smoothing effect on the initial estimate with a two-stage location estimation architecture [16], [17]. Simulation results illustrate that the proposed GAL-KF scheme can achieve higher accuracy for the MS's estimated location compared to the other existing methods in both line-of-sight (LOS) and none-line-of-sight (NLOS) environments.

The contributions of proposed GAL algorithms are summarized as follows: note that the conference version of this paper [18] introduces initial idea of fictitious BS rotation based on the geometric condition between the MS and BSs. In this paper, we extend this concept to several aspects as follows: comprehensive geometric properties between the BSs and MS are first analyzed in the presence of linearization loss. The benefits of fictitious BS rotation within the GAL algorithms can be observed from the analysis of geometric properties between the BSs and MS. Based on the concept of fictitious BS rotation, the proposed GAL algorithms decouple the original LEP into 1) an L-LEP with closed form solution and 2) the remaining nonlinear part as the fictitiously moveable BS problem. The L-LEP can be efficiently solved by the two-step LS estimator to provide an initial estimation for the fictitiously moveable BS problem. Note that the cost function of fictitiously movable BS problem is basically a mixture of trigonometric functions depending on the geometric configuration between the MS and BSs. Therefore, the peak value of cost function can be obtained with low computational complexity. In other words, the GAL algorithms decouple the original problem into two subproblems with efficient computation; while it can still provides better performance compared to the other existing nonlinear methods.

The remainder of this paper is organized as follows: Section 2 describes the properties that are derived from the CRLB and the L-CRLB metrics. The determination of fictitious BS's locations based on the proposed GAL algorithm is explained in Section 3; while Section 4 demonstrates the GAL-TSLS and the GAL-KF schemes as the implementation of the GAL algorithm. Section 5 shows the performance evaluation of the proposed schemes. The conclusions are drawn in Section 6.

## 2 Analysis of CRLB and L-CRLB

### 2.1 Mathematical Modeling of Signal Sources

The signal model for the TOA measurements is adopted for two-dimensional (2D) location estimation. The set $\boldsymbol{r}$ contains all the available measured relative distance, i.e., $\boldsymbol{r} = [r_1, \ldots, r_i, \ldots, r_N]$ where $N$ denotes the number of available BSs. The measured relative distance between the MS and the $i$th BS can be represented as

$$r_i = c \cdot t_i = \zeta_i + n_i \qquad \text{for } i = 1, 2, \ldots, N, \tag{1}$$

where $c$ is the speed of light. The parameter $t_i$ indicates the TOA measurement obtained from the $i$th BS, which is contaminated with the measurement noise $n_i$. The noiseless relative distance $\zeta_i$ in (1) between the MS's true position and the $i$th BS can be acquired as

$$\zeta_i = \|\boldsymbol{x} - \boldsymbol{x}_i\| \qquad \text{for } i = 1, 2, \ldots, N, \tag{2}$$

where $\boldsymbol{x} = [x, y]^T$ represents the MS's true position and $\boldsymbol{x}_i = [x_i, y_i]^T$ is the location of the $i$th BS. The notation $\|.\|$ denotes the euclidean norm of a vector and $[.]^T$ represents the transpose operator.

**Definition 1 (BS's Orientation).** *Considering the MS as a vertex in geometry, the orientation of $i$th BS ($\alpha_i$) is defined as the angle between the MS to the $i$th BS and the positive $x$-axis. Without loss of generality, the index $i$ of BSs are sorted such that the $i$th BS is located at the angle $\alpha_1 \leq \alpha_2 \leq \cdots \alpha_i \cdots \leq \alpha_N$ for $i = 1$ to $N$.*

Based on the definition of $\alpha_i$, the following geometric relationship can also be obtained as $\cos\alpha_i = (x_i - x)/\zeta_i$ and $\sin\alpha_i = (y_i - y)/\zeta_i$.

### 2.2 Properties of CRLB

**Definition 2 (Location Estimation Problem).** *By collecting the measurements $\boldsymbol{r}$, the goal of the LEP is to generate a 2D estimate $\hat{\boldsymbol{x}} = [\hat{x}, \hat{y}]^T$ of the MS's location.*

The CRLB represents the theoretical lowest error variance of an unknown parameter for any unbiased estimator. Note that the CRLB in the rest of this paper refers to the CRLB for the conventional LEP. Therefore, based on the TOA-based LEP as in (1) and (2), the variance of the MS's estimated position $\hat{\boldsymbol{x}}$ will be greater or equal to the CRLB ($\mathcal{C}$) as

$$E\{\|\hat{\boldsymbol{x}} - \boldsymbol{x}\|^2\} \geq \mathcal{C} = [\mathbf{I}_{\boldsymbol{x}}^{-1}]_{11} + [\mathbf{I}_{\boldsymbol{x}}^{-1}]_{22}, \tag{3}$$

where the CRLB $\mathcal{C} = [\mathbf{I}_{\boldsymbol{x}}^{-1}]_{11} + [\mathbf{I}_{\boldsymbol{x}}^{-1}]_{22}$ inherently represents the theoretical minimum mean square error (MMSE) of position. It is noted that $[\mathbf{I}_{\boldsymbol{x}}^{-1}]_{11}$ and $[\mathbf{I}_{\boldsymbol{x}}^{-1}]_{22}$ correspond to the first and second diagonal terms of the inverse of $2 \times 2$ FIM $\mathbf{I}_{\boldsymbol{x}}$, which can be obtained as

$$\mathbf{I}_{\boldsymbol{x}} = \mathbf{G} \cdot \mathbf{I}_{\boldsymbol{\zeta}} \cdot \mathbf{G}^T, \tag{4}$$

where

$$\mathbf{G} = \frac{\partial \boldsymbol{\zeta}}{\partial \boldsymbol{x}} = \begin{bmatrix} \frac{x_1 - x}{\zeta_1} & \cdots & \frac{x_i - x}{\zeta_i} & \cdots & \frac{x_N - x}{\zeta_N} \\ \frac{y_1 - y}{\zeta_1} & \cdots & \frac{y_i - y}{\zeta_i} & \cdots & \frac{y - y_N}{\zeta_N} \end{bmatrix} \tag{5}$$

$$= \begin{bmatrix} \cos\alpha_1 & \cdots & \cos\alpha_i & \cdots & \cos\alpha_N \\ \sin\alpha_1 & \cdots & \sin\alpha_i & \cdots & \sin\alpha_N \end{bmatrix}, \tag{6}$$

$$\mathbf{I}_{\boldsymbol{\zeta}} = E\left[\frac{\partial}{\partial \boldsymbol{\zeta}} \ln f(\boldsymbol{r}|\boldsymbol{\zeta}) \cdot \left(\frac{\partial}{\partial \boldsymbol{\zeta}} \ln f(\boldsymbol{r}|\boldsymbol{\zeta})\right)^T\right]. \tag{7}$$

The $f(\boldsymbol{r}|\boldsymbol{\zeta})$ function in (7) denotes the probability density function for $\boldsymbol{r}$ conditioning on $\boldsymbol{\zeta}$, where $\boldsymbol{\zeta} = [\zeta_1, \ldots, \zeta_i, \ldots, \zeta_N]$. The matrices $\mathbf{G}$ and $\mathbf{I}_{\boldsymbol{\zeta}}$ are introduced as the change of variables since $\mathbf{I}_{\boldsymbol{x}}$ is unobtainable owing to the unknown MS's true position $\boldsymbol{x}$.

**Lemma 1.** *Considering the TOA-based LEP, the noise model for each measurement $r_i$ is an i.i.d. Gaussian distribution with zero mean and a fixed set of variances $\sigma_{r_i}^2$ as $n_i \sim \mathcal{N}(0, \sigma_{r_i}^2)$. The minimum CRLB $\mathcal{C}_m$ with respect to the angle $\alpha_i$ can be achieved in [13] as*

$$\mathcal{C}_m = \frac{4}{\sum_{i=1}^{N} \frac{1}{\sigma_{r_i}^2}}, \tag{8}$$

*if the following two conditions hold:*

$$\begin{cases} \sum_{i=1}^{N} \frac{1}{\sigma_{r_i}^2} \sin 2\alpha_i = 0, \\ \sum_{i=1}^{N} \frac{1}{\sigma_{r_i}^2} \cos 2\alpha_i = 0. \end{cases} \tag{9}$$

**Proof.** Based on (1), $f(\boldsymbol{r}|\boldsymbol{\zeta})$ can be obtained as

$$f(\boldsymbol{r}|\boldsymbol{\zeta}) \propto \prod_{i=1}^{N} \exp\left[-\frac{1}{2\sigma_{r_i}^2}(r_i - \zeta_i)^2\right]. \tag{10}$$

Therefore, the matrix $\mathbf{I}_{\boldsymbol{\zeta}}$ can be derived from (7) as $\mathbf{I}_{\boldsymbol{\zeta}} = \mathrm{diag}\{[\sigma_{r_1}^{-2}, \sigma_{r_2}^{-2}, \ldots, \sigma_{r_i}^{-2}, \ldots, \sigma_{r_N}^{-2}]\}$. The $2 \times 2$ matrix $\mathbf{I}_{\boldsymbol{x}}$ can be obtained from (4) and (7) as

$$\begin{aligned} \mathbf{I}_{\boldsymbol{x}} &= \begin{bmatrix} [\mathbf{I}_{\boldsymbol{x}}]_{11} & [\mathbf{I}_{\boldsymbol{x}}]_{12} \\ [\mathbf{I}_{\boldsymbol{x}}]_{21} & [\mathbf{I}_{\boldsymbol{x}}]_{22} \end{bmatrix} \\ &= \begin{bmatrix} \sum_{i=1}^{N} \frac{1}{\sigma_{r_i}^2} \cos^2\alpha_i & \sum_{i=1}^{N} \frac{1}{\sigma_{r_i}^2} \cos\alpha_i \cdot \sin\alpha_i \\ \sum_{i=1}^{N} \frac{1}{\sigma_{r_i}^2} \cos\alpha_i \cdot \sin\alpha_i & \sum_{i=1}^{N} \frac{1}{\sigma_{r_i}^2} \sin^2\alpha_i \end{bmatrix}. \end{aligned} \tag{11}$$

In order to obtain the minimum CRLB, (3) can further be derived as

$$\begin{aligned} E\{(\hat{\boldsymbol{x}} - \boldsymbol{x})^2\} &\geq \left[\mathbf{I}_{\boldsymbol{x}}^{-1}\right]_{11} + \left[\mathbf{I}_{\boldsymbol{x}}^{-1}\right]_{22} = \frac{[\mathbf{I}_{\boldsymbol{x}}]_{11} + [\mathbf{I}_{\boldsymbol{x}}]_{22}}{[\mathbf{I}_{\boldsymbol{x}}]_{11} \cdot [\mathbf{I}_{\boldsymbol{x}}]_{22} - [\mathbf{I}_{\boldsymbol{x}}]_{12}^2} \\ &\geq \frac{[\mathbf{I}_{\boldsymbol{x}}]_{11} + [\mathbf{I}_{\boldsymbol{x}}]_{22}}{[\mathbf{I}_{\boldsymbol{x}}]_{11} \cdot [\mathbf{I}_{\boldsymbol{x}}]_{22}}. \end{aligned} \tag{12}$$

Noted that the second inequality in (12) is valid since the quadratic term $[\mathbf{I}_{\boldsymbol{x}}]_{12}^2 \geq 0$ for all $\alpha_i$. Therefore, one of the necessary conditions to achieve minimum CRLB will be $[\mathbf{I}_{\boldsymbol{x}}]_{12} = \sum_{i=1}^{N} \frac{1}{\sigma_{r_i}^2} \cos\alpha_i \cdot \sin\alpha_i = 0$, which validates the first equation of (9). Moreover, since $\cos^2\alpha_i + \sin^2\alpha_i = 1$ for all $\alpha_i$, the numerator in (12) becomes $[\mathbf{I}_{\boldsymbol{x}}]_{11} + [\mathbf{I}_{\boldsymbol{x}}]_{22} = \sum_{i=1}^{N} 1/\sigma_{r_i}^2$. Consequently, to acquire the minimum value of CRLB corresponds to maximizing the denominator $[\mathbf{I}_{\boldsymbol{x}}]_{11} \cdot [\mathbf{I}_{\boldsymbol{x}}]_{22}$ in (12). According to the *inequality of arithmetic and geometric means*, the following relationship can be obtained:

$$\sqrt{[\mathbf{I}_{\boldsymbol{x}}]_{11} \cdot [\mathbf{I}_{\boldsymbol{x}}]_{22}} \leq \frac{[\mathbf{I}_{\boldsymbol{x}}]_{11} + [\mathbf{I}_{\boldsymbol{x}}]_{22}}{2} = \frac{1}{2} \sum_{i=1}^{N} \frac{1}{\sigma_{r_i}^2}, \tag{13}$$

where the equality holds if and only if $[\mathbf{I}_{\boldsymbol{x}}]_{11} = [\mathbf{I}_{\boldsymbol{x}}]_{22}$, which corresponds to the second equation in (9). By substituting (13) into (12), the minimum CRLB can be obtained as $\mathcal{C}_m = 4/(\sum_{i=1}^{N} \frac{1}{\sigma_{r_i}^2})$. This completes the proof. □

**Example 1 (Network Layout with Minimum CRLB).** Following the requirement as in Lemma 1 with $N = 3$ and all the variances are equivalent $\sigma_{r_i}^2 = \sigma_r^2$ for $i = 1$ to 3, the best geometric layout that can achieve the minimum CRLB $\mathcal{C}_m = 4\sigma_r^2/3$ is acquired at either the angle sets $\{\alpha_1, \alpha_2, \alpha_3\} = \{\gamma,\ \gamma + 120^\circ,\ \gamma + 240^\circ\}$ or $\{\alpha_1, \alpha_2, \alpha_3\} = \{\gamma, \gamma + 60^\circ, \gamma + 120^\circ\} \forall \gamma = [0^\circ, 360^\circ)$.

### 2.3 Properties of Proposed L-CRLB

**Definition 3 (Linearized Location Estimation Problem).** *In order to estimate the MS's position $\boldsymbol{x}$, the nonlinear terms $x^2$ and $y^2$ in (2) are replaced by a new parameter $R = x^2 + y^2$. The goal of the L-LEP is to generate an estimate $\hat{\boldsymbol{\theta}} = [\hat{x}_L, \hat{y}_L, \hat{R}]^T$ based on the collecting measurements $\boldsymbol{r}$.*

Note that the MS's estimated position $\hat{\boldsymbol{x}}_L = [\hat{x}_L, \hat{y}_L]^T$ of the L-LEP is in general not optimal compared to the original LEP since an additional nonlinear parameter $R$ is also estimated, which reduces the estimation precision for $\hat{\boldsymbol{x}}_L$ under fixed set of measurement inputs. This intuitive

observation explains that the conventional CRLB cannot be achieved by the linearized location estimator for LEP. In order to appropriately describe the behavior of linearized location estimator, the L-CRLB is defined based on the relationships in (1) and (2) as follows:

**Definition 4 (L-CRLB).** *The L-CRLB ($\mathcal{C}_L$) is defined for linearized location estimation in terms of the estimated parameters $\hat{\boldsymbol{x}}_L$ as*

$$E\{\|\hat{\boldsymbol{x}}_L - \boldsymbol{x}\|^2\} \geq \mathcal{C}_L = [\mathbf{I}_{\boldsymbol{\theta}}^{-1}]_{11} + [\mathbf{I}_{\boldsymbol{\theta}}^{-1}]_{22}, \tag{14}$$

*where $[\mathbf{I}_{\boldsymbol{\theta}}^{-1}]_{11}$ and $[\mathbf{I}_{\boldsymbol{\theta}}^{-1}]_{22}$, respectively, denotes the first and second diagonal terms of the inverse of $3 \times 3$ FIM matrix $\mathbf{I}_{\boldsymbol{\theta}}$ as*

$$\mathbf{I}_{\boldsymbol{\theta}} = \mathbf{H} \cdot \mathbf{I}_{\zeta} \cdot \mathbf{H}^T, \tag{15}$$

*with*

$$\mathbf{H} = \frac{\partial \zeta}{\partial \boldsymbol{\theta}} = \begin{bmatrix} \cos\alpha_1 & \cdots & \cos\alpha_i & \cdots & \cos\alpha_N \\ \sin\alpha_1 & \cdots & \sin\alpha_i & \cdots & \sin\alpha_N \\ \dfrac{1}{2\zeta_1} & \cdots & \dfrac{1}{2\zeta_i} & \cdots & \dfrac{1}{2\zeta_N} \end{bmatrix}, \tag{16}$$

*and $\mathbf{I}_{\zeta}$ obtained from (7).*

Note that the derivation of the inequality (14) is neglected in this paper, which can be similarly referred from the derivation of CRLB in [19]. Based on the theory of CRLB, the closed forms of FIM in (15) can be formulated and the relevant matrix in (16) is derived. In other words, the proposed L-CRLB is adopted to denote the minimum variance for any estimator that estimates the parameter vector $\boldsymbol{\theta}$ from the TOA measurements. In the following lemma, the fact that the L-CRLB is greater than or equal to the CRLB will be proved.

**Lemma 2.** *Considering that there exists sufficient measurement inputs for location estimation with zero mean Gaussian noises, the L-CRLB is greater than or equal to the CRLB, i.e., $\mathcal{C}_L \geq \mathcal{C}$.*

**Proof.** The $3 \times 3$ matrix $\mathbf{I}_{\boldsymbol{\theta}}$ can be obtained from (7) and (15) as

$$\mathbf{I}_{\boldsymbol{\theta}} = \begin{bmatrix} \mathbf{I}_{\boldsymbol{x}} & \mathbf{B} \\ \mathbf{B}^T & \mathbf{C} \end{bmatrix}, \tag{17}$$

where the matrices

$$\mathbf{B} = \begin{bmatrix} \sum_{i=1}^{N} \dfrac{1}{\sigma_{r_i}^2} \dfrac{\cos\alpha_i}{2\zeta_i} & \sum_{i=1}^{N} \dfrac{1}{\sigma_{r_i}^2} \dfrac{\sin\alpha_i}{2\zeta_i} \end{bmatrix}^T$$

and

$$\mathbf{C} = \left[ \sum_{i=1}^{N} \frac{1}{4\sigma_{r_i}^2 \zeta_i^2} \right].$$

Note that the $2 \times 2$ matrix $\mathbf{I}_{\boldsymbol{x}}$ is the same as that obtained from (4). Moreover, the inverse of the covariance matrix $\mathbf{I}_{\boldsymbol{\theta}}$ can be represented as

$$\mathbf{I}_{\boldsymbol{\theta}}^{-1} = \begin{bmatrix} [\mathbf{I}_{\boldsymbol{\theta}}]_{2\times 2}^{-1} & \mathbf{B}' \\ \mathbf{B}'^T & \mathbf{C}' \end{bmatrix}, \tag{18}$$

where the $2\times 2$ submatrix $[\mathbf{I}_{\boldsymbol{\theta}}]_{2\times 2}^{-1}$ of $\mathbf{I}_{\boldsymbol{\theta}}^{-1}$ can be obtained as $[\mathbf{I}_{\boldsymbol{\theta}}]_{2\times 2}^{-1} = (\mathbf{I}_{\boldsymbol{x}} - \mathbf{B} \cdot \mathbf{C}^{-1} \cdot \mathbf{B}^T)^{-1}$ based on the matrix inversion lemma. Considering that there are sufficient measurement inputs for the linearized location estimation, i.e., $N \geq 3$, both the covariance matrices $\mathbf{I}_{\boldsymbol{\theta}}$ and $\mathbf{I}_{\boldsymbol{x}}$ are nonsingular which corresponds to positive definite matrices. Consequently, the submatrix $[\mathbf{I}_{\boldsymbol{\theta}}]_{2\times 2}$ and their corresponding inverse matrices $\mathbf{I}_{\boldsymbol{\theta}}^{-1}$, $\mathbf{I}_{\boldsymbol{x}}^{-1}$, and $[\mathbf{I}_{\boldsymbol{\theta}}]_{2\times 2}^{-1}$ are positive definite. Furthermore, both $\mathbf{C}$ and $\mathbf{C}^{-1}$ are positive definite since

$$\mathbf{C} = \left[ \sum_{i=1}^{N} \frac{1}{4\sigma_{r_i}^2 \zeta_i^2} \right] > 0.$$

Therefore, it can be shown that $[\mathbf{I}_{\boldsymbol{\theta}}]_{2\times 2} = (\mathbf{I}_{\boldsymbol{x}} - \mathbf{B} \cdot \mathbf{C}^{-1} \cdot \mathbf{B}^T) \leq \mathbf{I}_{\boldsymbol{x}}$ since $\mathbf{C}^{-1}$ is positive definite and the equality only occurs with zero matrix $\mathbf{B}$. Given two positive definite matrices $[\mathbf{I}_{\boldsymbol{\theta}}]_{2\times 2}$ and $\mathbf{I}_{\boldsymbol{x}}$, $\mathbf{I}_{\boldsymbol{x}} \geq [\mathbf{I}_{\boldsymbol{\theta}}]_{2\times 2}$ if and only if $[\mathbf{I}_{\boldsymbol{\theta}}]_{2\times 2}^{-1} \geq \mathbf{I}_{\boldsymbol{x}}^{-1} > 0$. Furthermore, since $[\mathbf{I}_{\boldsymbol{\theta}}]_{2\times 2}^{-1} \geq \mathbf{I}_{\boldsymbol{x}}^{-1}$, their corresponding traces will follow as trace $([\mathbf{I}_{\boldsymbol{\theta}}]_{2\times 2}^{-1}) \geq$ trace $(\mathbf{I}_{\boldsymbol{x}}^{-1})$ which consequently results in $[\mathbf{I}_{\boldsymbol{\theta}}]_{11}^{-1} + [\mathbf{I}_{\boldsymbol{\theta}}]_{22}^{-1} \geq [\mathbf{I}_{\boldsymbol{x}}]_{11}^{-1} + [\mathbf{I}_{\boldsymbol{x}}]_{22}^{-1}$. This completes the proof. □

**Corollary 1.** *The L-CRLB is equivalent to the CRLB if the following two conditions hold*

$$\begin{cases} \sum_{i=1}^{N} \dfrac{1}{\sigma_{r_i}^2} \dfrac{\sin\alpha_i}{\zeta_i} = 0, \\ \sum_{i=1}^{N} \dfrac{1}{\sigma_{r_i}^2} \dfrac{\cos\alpha_i}{\zeta_i} = 0. \end{cases} \tag{19}$$

**Proof.** As stated in Lemma 2, the necessary and sufficient condition for both L-CRLB and CRLB to be equivalent is that $\mathbf{B}$ is a zero matrix. Therefore, the two matrix elements in $\mathbf{B}$, i.e., $\sum_{i=1}^{N} \cos\alpha_i/(\sigma_{r_i}^2 \zeta_i)$ and $\sum_{i=1}^{N} \sin\alpha_i/(\sigma_{r_i}^2 \zeta_i)$, will be equal to zero. □

It can be generalized from Corollary 1 that the two error terms $\varepsilon_1 = \sum_{i=1}^{N} \cos\alpha_i/(\sigma_{r_i}^2 \zeta_i)$ and $\varepsilon_2 = \sum_{i=1}^{N} \sin\alpha_i/(\sigma_{r_i}^2 \zeta_i)$ will influence the value of L-CRLB, which consequently affect the precision of linearized location estimators. Under the geometric layout with smaller values of $\varepsilon_1$ and $\varepsilon_2$, smaller difference between the CRLB and L-CRLB value can be obtained, which indicates that the linearization loss by adopting linearized location estimators is smaller. $\varepsilon_1$ and $\varepsilon_2$ can be mapping to the $x$- and $y$-direction vectors from the MS to the BS. The noise variance terms can be regarded as the weighting of the direction vector. The minimum linearization loss for the linearized location estimator is achieved when the sum of the weighted direction vector from the MS to the BS is equal to zero. Besides, consider the case that the MS is situated outside of the polygon formed by the BSs, all the angles $\alpha_i$ will be in the range of $[0, 180°]$ which results in larger value of the error terms $\varepsilon_1$ and $\varepsilon_2$. As a result, the estimation errors acquired from the linearized location estimator will be comparably large in this type of geometric relationship. The following example is given to demonstrate the scenario where the L-CRLB is equal to CRLB.

**Example 2 (Network Layout for Equivalent L-CRLB and CRLB).** Assuming that the variances $\sigma_{r_i}$ from all the measurement noises are equivalent, the L-CRLB can achieve the CRLB if 1) the noiseless distances $\zeta_i$ from the MS to all the corresponding BSs are equal, and 2) the orientation angles $\alpha_i$ from the MS to all the BSs are uniformly distributed in $[0^\circ, 360^\circ)$ as $\alpha_i = 360^\circ \cdot (i-1)/N + \gamma$, $\forall \gamma = [0^\circ, 360^\circ)$ and $i = 1$ to $N$.

**Proof.** By substituting the conditions $\zeta_1 = \zeta_2 = \cdots = \zeta_N$ and $\sigma_{r_1} = \sigma_{r_2} = \cdots = \sigma_{r_N}$ into (19), the necessary condition for the L-CRLB and the CRLB to be equivalent becomes $\sum_{i=1}^{N} \cos\alpha_i = 0$ and $\sum_{i=1}^{N} \sin\alpha_i = 0$. Based on the assumptions as stated above, a vector can be utilized to represent the distance from the MS to the $i$th BS as $\nu_i = [\cos\alpha_i, \sin\alpha_i]$ for $i = 1$ to $N$. In order to satisfy the conditions for both $\sum_{i=1}^{N} \cos\alpha_i = 0$ and $\sum_{i=1}^{N} \sin\alpha_i = 0$, the summation for projecting all unit vectors $\nu_i$ for $i = 1$ to $N$ on the $x$-axis and $y$-axis respectively should be equal to zero. In order to achieve this condition, it can be verified that the angles $\alpha_i$ will be uniformly distributed in $[0^\circ, 360^\circ)$ with its value equal to $\alpha_i = 360^\circ \cdot (i-1)/N + \gamma$, $\forall \gamma = [0^\circ, 360^\circ)$. This completes the proof. □

**Corollary 2.** *The minimum L-CRLB ($\mathcal{C}_{L,m}$) is achieved if the conditions stated in (9) and (19) are satisfied.*

**Proof.** It has been indicated that the minimum CRLB ($\mathcal{C}_m$) can be obtained if the conditions in (9) hold. Moreover, Corollary 1 proves that (19) should be satisfied for both L-CRLB and CRLB to be equivalent. Therefore, the minimum L-CRLB ($\mathcal{C}_{L,m}$) can be achieved if (9) and (19) are satisfied. □

It can be observed from Corollary 2 that additional condition (19) should be satisfied for achieving minimum L-CRLB comparing with the minimum CRLB. The major difference is that the CRLB is affected by the angles $\alpha_i$ and signal variances $\sigma_{r_i}^2$; while the L-CRLB additionally depends on the distance information $\zeta_i$. Therefore, the performance of the L-LEP is affected by the additional relative distance information between the MS and BSs. In order to provide intuitive explanation, the exemplified network layout for achieving minimum L-CRLB is shown as follows.

**Example 3 (Network Layout with Minimum L-CRLB).** Following the requirement as in Lemmas 1 and 2 with $N = 3$ and all the variances are equivalent, i.e., $\sigma_{r_i}^2 = \sigma_r^2$ for $i = 1$ to 3, and further assuming that the noiseless distances $\zeta_i$ from the MS to all the three BSs are equivalent, the minimum L-CRLB can be achieved only at the angle sets $\{\alpha_1, \alpha_2, \alpha_3\} = \{\gamma, \gamma + 120^\circ, \gamma + 240^\circ\} \forall\ \gamma = [0^\circ, 360^\circ)$.

**Proof.** Considering $N = 3$ and $\sigma_{r_1} = \sigma_{r_2} = \sigma_{r_3} = \sigma_r$ in (9), the following relationship is obtained:

$$\begin{cases} \sin 2\alpha_1 + \sin 2\alpha_2 + \sin 2\alpha_3 = 0, \\ \cos 2\alpha_1 + \cos 2\alpha_2 + \cos 2\alpha_3 = 0. \end{cases} \tag{20}$$

It can be verified that both conditions in (20) are only satisfied at either one of the following angle sets: $\{\alpha_1, \alpha_2, \alpha_3\} = \{\gamma, \gamma + 120^\circ, \gamma + 240^\circ\}$ and $\{\alpha_1, \alpha_2, \alpha_3\} = \{\gamma, \gamma + 60^\circ, \gamma + 120^\circ\} \forall \gamma = [0^\circ, 360^\circ)$. The corresponding minimum CRLB can be calculated from (8) as $\mathcal{C}_m = 4\sigma_r^2/3$.

On the other hand, according to Corollary 2, the conditions (9) and (19) must be satisfied in order to achieve minimum L-CRLB. Considering the $N = 3$ case with $\zeta_1 = \zeta_2 = \zeta_3$, condition (19) is rewritten as

$$\begin{cases} \sin\alpha_1 + \sin\alpha_2 + \sin\alpha_3 = 0, \\ \cos\alpha_1 + \cos\alpha_2 + \cos\alpha_3 = 0. \end{cases} \tag{21}$$

It can be verified that only the angle sets $\{\alpha_1, \alpha_2, \alpha_3\} = \{\gamma, \gamma + 120^\circ, \gamma + 240^\circ\} \forall\ \gamma = [0^\circ, 360^\circ)$ can satisfy all the three conditions as defined in (20) and (21) for achieving the minimum value of L-CRLB. This completes the proof. □

In other words, when the MS is positioned at the center of a regular polygon formed by the BSs, the proposed L-CRLB will be equivalent to the CRLB based on the conditions stated in (19). Example 3 describes the fact that minimum CRLB can be achieved under two different set of orientation angles; while the minimum L-CRLB is reached by one of its subset of angles. This indicates the situation that the L-CRLB provides a more stringent criterion compared to the CRLB for achieving its minimum value. Even though certain network layouts are suggested to achieve minimum CRLB, it does not guarantee that the corresponding L-CRLB can reach the same value. Therefore, the CRLB does not provide sufficient information to be used as the criterion for the linearized location estimator of the L-LEP; while the L-CRLB can be more feasible to reveal the geometric properties and requirements.

**Example 4 (Contour Plots of CRLB and L-CRLB).** In order to observe the difference between the CRLB and L-CRLB, their corresponding contour plots under the number of BSs $N = 3$ are shown in Figs. 1a and 1b, respectively. Note that the three BSs are located at the vertexes of a regular triangular which are denoted with red circles in Figs. 1a and 1b. The positions of BSs are $\boldsymbol{x}_1 = [300, 200]^T$ with $\alpha_1 = 0^\circ$, $\boldsymbol{x}_2 = [150, 286.6]^T$ with $\alpha_2 = 120^\circ$, and $\boldsymbol{x}_3 = [150, 113.4]^T$ with $\alpha_3 = 240^\circ$. Based on the three BS's positions, each individual contour point represents the corresponding CRLB or L-CRLB value when the MS is situated at that location. The standard deviation of measurement noises $\sigma_{r_i}$ is chosen as 1 m for simplicity. It can be observed from Fig. 1a that there are four minimum points for the CRLB value equal to $\mathcal{C}_m = 1.33$ with MS's positions as $\boldsymbol{x} = [200, 200]^T$, $[100, 200]^T$, $[260, 120]^T$, and $[260, 280]^T$. The conditions for minimum CRLB can be verified by substituting the corresponding parameters into the condition (9). The minimum CRLB value can also be validated to satisfy (8), which demonstrates the correctness of Lemma 1.

On the other hand, by comparing Figs. 1a and 1b, it is observed that the distribution of L-CRLB is different from that of CRLB. The only minimum L-CRLB value identical to that of the CRLB, i.e., $\mathcal{C}_{L,m} = \mathcal{C}_m = 1.33$, is located at the center of regular triangle formed by the three BSs, i.e., $\boldsymbol{x} = [200, 200]^T$. Starting at the MS's position with minimum L-CRLB, the L-CRLB value will increase in all directions. Except for the minimum L-CRLB at the center of the triangle, the relationship that $\mathcal{C}_L > \mathcal{C}$ can be observed from both Figs. 1a and 1b. Moreover, the difference between the L-CRLB and CRLB inside the triangle is smaller than that outside of the triangle. The reason can be contributed to the estimation

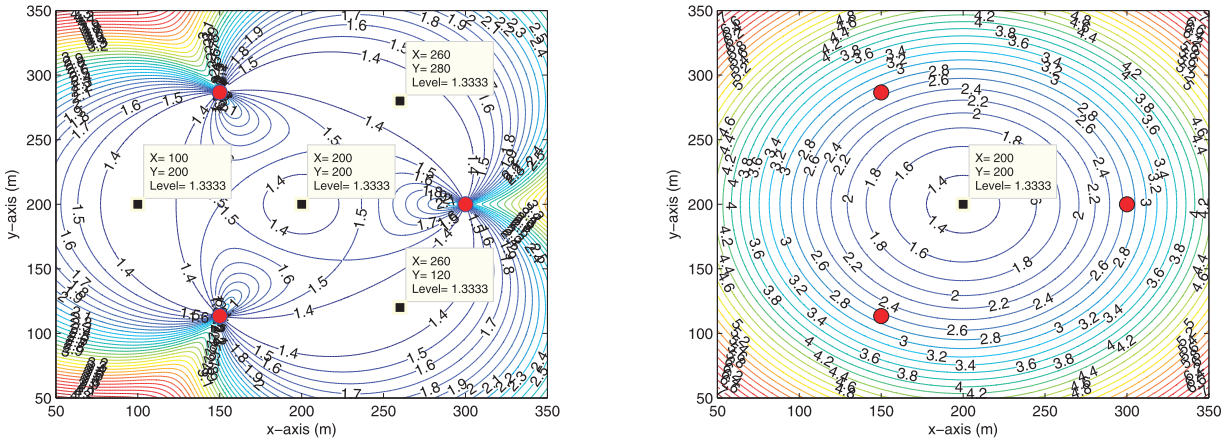


Fig. 1. (a) CRLB contour under $N = 3$. (b) L-CRLB contour under $N = 3$. Red circles denote the positions of BSs.

of parameter $R$ by adopting the L-CRLB criterion, which introduces the two terms $\varepsilon_1$ and $\varepsilon_2$. Owing to the nonlinear behavior of location estimation, the additional consideration of $R$ within the L-CRLB can better characterize the performance of linearized location estimator for the L-LEP. The correctness of minimum L-CRLB value obtained from Fig. 1b can also be verified by substituting corresponding parameters into the conditions stated in Lemma 2, i.e., the conditions (9) and (19) can all be satisfied. By comparing the results from Figs. 1a and 1b, Corollaries 1 to 2 and Examples 2 to 3 can all be validated by substituting the corresponding numerical values.

In order to provide better explanation on the properties of CRLB and L-CRLB, the definitions of several geometric relationships between the MS and the BSs are described as follows: note that Fig. 2 illustrates the BS's orientation for Definition 1 and geometric relationship between BSs and MS for Definitions 5 to 8.

**Definition 5 (BS's Adjacent Included Angle).** *Based on the BS's orientation $\alpha_i$, the adjacent included angle between two neighboring ith and $(i+1)$th BSs is defined as $\beta_i = \alpha_{i+1} - \alpha_i$ for $i = 1$ to $N-1$, and $\beta_N = 360^\circ + \alpha_1 - \alpha_N$.*

**Definition 6 (BS Polygon).** *Considering the locations of BSs as the vertices in geometry, the BS polygon is defined by connecting the adjacent BSs as the edges of the polygon from $\mathrm{BS}_1$ to $\mathrm{BS}_N$.*

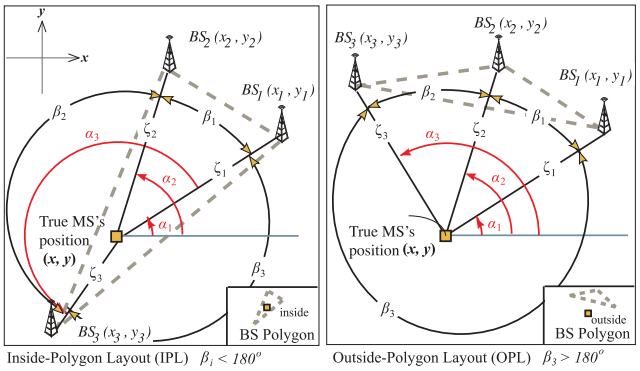


Fig. 2. Illustration for Definitions 5 to 8.

**Definition 7 (Inside-Polygon Layout (IPL)).** *Given the BS's adjacent included angle set $\boldsymbol{\beta} = \{\beta_1, \ldots, \beta_i, \ldots, \beta_N\}$, an inside-polygon layout is defined if the MS is located inside the BS polygon where $0^\circ < \beta_i < 180^\circ \ \forall\ i$ from 1 to $N$.*

**Definition 8 (Outside-Polygon Layout (OPL)).** *Given the BS's adjacent included angle set $\boldsymbol{\beta} = \{\beta_1, \ldots, \beta_i, \ldots, \beta_N\}$, a outside-polygon layout is defined if the MS is located outside the BS polygon where there exists an adjacent included angle $180^\circ \le \beta_i < 360^\circ \ \forall\ i$ from 1 to $N$.*

**Lemma 3.** *Consider two types of layouts, IPL and OPL, between the MS and three BSs under the requirements with equivalent variances $\sigma_{r_i}^2$ and noiseless distances $\zeta_i$ for $i = 1$ to 3. There can exist both IPL and OPL that possess the same CRLB value; while the corresponding L-CRLB value of the IPL is smaller than that of the OPL.*

**Proof.** Given an IPL, the set of BS's adjacent included angle is defined as $\boldsymbol{\beta}_{in} = \{\beta_1, \beta_2, \beta_3 = 360^\circ - \beta_1 - \beta_2\}$ where $0^\circ < \beta_i < 180^\circ \ \forall\ i = 1$ to 3. The set of BS's orientation between the MS and three BSs can be represented as $\boldsymbol{\alpha}_{in} = \{\alpha_1 = 0, \alpha_2 = \beta_1, \alpha_3 = \beta_1 + \beta_2\}$. Without lose of generality, $\alpha_1$ is set with zero degree according to the rotation property as proven in [13] for CRLB. In order to establish an OPL, the third BS is repositioned to the reflected side with respect to the MS, which results in its BS's orientation as $\boldsymbol{\alpha}_{out} = \{\alpha_1 = 0, \alpha_2 = \beta_1, \alpha_3' = \beta_1 + \beta_2 - 180^\circ\}$. By substituting both IPL and OPL cases with $\boldsymbol{\alpha}_{in} = \{0, \alpha_2, \alpha_3\}$ and $\boldsymbol{\alpha}_{out} = \{0, \alpha_2, \alpha_3 - 180^\circ\}$ respectively into (3), it can be observed that same value of CRLB is achieved by both OPL and OPL.

Moreover, in order to compare the L-CRLB for the IPL and OPL, i.e., $\mathcal{C}_{L,in}$ and $\mathcal{C}_{L,out}$, the difference of L-CRLB for both layouts is derived from (14) to (16) with the substitution of $\boldsymbol{\alpha}_{in}$ and $\boldsymbol{\alpha}_{out}$ as

$$\begin{aligned}\delta &= \mathcal{C}_{L,in} - \mathcal{C}_{L,out} = [\mathbf{I}_{\theta,in}]_{11}^{-1} + [\mathbf{I}_{\theta,in}]_{22}^{-1} - [\mathbf{I}_{\theta,out}]_{11}^{-1} - [\mathbf{I}_{\theta,out}]_{22}^{-1} \\ &= \frac{1}{D_{\mathbf{I}_{\theta,in}} D_{\mathbf{I}_{\theta,out}}} \left\{ -8 \cos\frac{\alpha_2}{2} \cos\frac{2\alpha_3 - \alpha_2}{2} (1 - \cos\alpha_2) \right. \\ &\quad \left. \cdot \left[ 2\cos\alpha_2 + 2\cos\alpha_3 \cos(\alpha_2 - \alpha_3) - 4 \right] \right\}, \end{aligned} \tag{22}$$

where $D_{\mathbf{I}_{\theta,in}}$ and $D_{\mathbf{I}_{\theta,out}}$ denote the determinants of the FIM matrix $\mathbf{I}_{\theta,in}$ and $\mathbf{I}_{\theta,out}$ for the L-CRLB of IPL and OPL respectively. Since both $\mathbf{I}_{\theta,in}$ and $\mathbf{I}_{\theta,out}$ are positive definite, their corresponding determinants $D_{\mathbf{I}_{\theta,in}}$ and $D_{\mathbf{I}_{\theta,out}}$ will be positive values. Furthermore, the following conditions hold since the BS's orientation set $\boldsymbol{\alpha}_{in}$ corresponds to an IPL: $0^\circ < \alpha_2 < 180^\circ$, $0^\circ < \alpha_3 - \alpha_2 < 180^\circ$, and $180^\circ < \alpha_3 < 360^\circ$. Therefore, the following conditions hold for the numerator terms in (22): $\cos(\alpha_2/2) > 0$ since $0^\circ < \alpha_2/2 < 90^\circ$, $\cos[(2\alpha_3 - \alpha_2)/2] < 0$ since $90^\circ < (2\alpha_3 - \alpha_2)/2 < 270^\circ$, $(1 - \cos\alpha_2) > 0$ since $-1 < \cos\alpha_2 < 1$, and $2\cos\alpha_2 + 2\cos\alpha_3\cos(\alpha_2 - \alpha_3) < 4$ since $-1 < \cos\alpha_2 < 1$ and $-1 < \cos\alpha_3\cos(\alpha_2 - \alpha_3) < 1$. As a consequence, the difference $\delta = \mathcal{C}_{L,in} - \mathcal{C}_{L,out} < 0$ which corresponds to the result that the L-CRLB of the IPL is smaller than that of the OPL. This completes the proof. □

A key contribution of this paper is obtained from Lemma 3 that the proposed L-CRLB can describe the geometric relationship between the MS and its corresponding BSs, i.e., either the IPL or OPL; while the conventional CRLB criterion observes the same value for both cases. It is found in Lemma 3 that the L-CRLB for MS to locate inside the BS polygon will be smaller than that for MS situated outside the BS polygon. This result implicitly indicates that the estimation accuracy from a linearized location estimator will be higher for the IPL compared to the OPL case. Based on this fact, the main objective of the remaining sections is to propose a localization algorithm to enhance the estimation accuracy of the linearized location estimator for the OPL.

## 3 Proposed Geometry-Assisted Localization Algorithm

The main objective of the proposed GAL scheme is to enhance the LLS-based algorithms by considering the geometric effect to the location estimation accuracy. The core component of the GAL scheme is to acquire the positions of the *fictitious* BSs to achieve the minimum L-CRLB value with respect to the MS's initial location estimate $\hat{\boldsymbol{x}}^o$. Note that the position of the $i$th fictitious BS with respect to the MS's initial location estimate can be represented based on the measurement distance $r_i$ and the BS's orientation $\alpha_i$. Since $r_i$ is available as the measured information, the determination of *fictitious* BS's position corresponds to the adjustment of the BS's orientation $\alpha_i$. The position information of these *fictitious* BSs will be utilized to replace that of the original BSs in order to achieve better geometric layout for location estimation, which will be discussed as the implementation of the GAL scheme in Section 4. In this section, the core mechanism of the GAL algorithm to identify which BSs should be fictitiously rotated will be demonstrated. The subschemes of the GAL algorithm with different numbers of fictitious BSs will be stated, i.e., the GAL with one fictitiously movable BS scheme (GAL(1BS)) and the GAL with two fictitiously movable BSs scheme (GAL(2BS)) in Sections 3.1 and 3.2, respectively. Section 3.3 describes the combined schemes of the GAL algorithm by selecting among different numbers of fictitious BSs based on the minimum L-CRLB requirement.

### 3.1 GAL with One Fictitiously Movable BS Scheme

The GAL(1BS) scheme is designed to fictitiously relocate the position of one BS according to the criterion for achieving the optimal geometric layout, i.e., the minimum L-CRLB. Note that only one BS is allowed to be fictitiously movable and the others remain fixed in this case. The objective of the GAL(1BS) scheme is to decide which BS should be fictitiously moved in order to obtain the minimum L-CRLB. The *GAL(1BS) problem* is defined as

$$\begin{aligned} j^m = \arg\min_{j=1,\ldots,N} \quad & \mathcal{C}_L\big(\tilde{\alpha}_j^m\big) \\ \text{subject to} \quad & \mathcal{C}_L\big(\tilde{\alpha}_j^m\big) < \mathcal{C}_L,\ j = 1,\ldots,N, \end{aligned} \tag{23}$$

where $\tilde{\alpha}_j^m$ represents the orientation of the $j^m$th fictitiously moveable BS that achieves the minimum L-CRLB. Providing that all the BSs within GAL(1BS) scheme cannot result in lowered L-CRLB values compared to the original $C_L$, the constraint defined in (23) will not be satisfied. In other words, the original L-CRLB has already been the lowest under the given measurement conditions, where none of the BSs is required to be fictitiously moved and the initial MS's location estimate will become the final estimate. By observing from the problem defined in (23), the optimal rotated angle $\tilde{\alpha}_j^m$ of a single BS should be determined first. The *one fictitiously movable BS problem* is defined to obtain the optimal rotated angle of the $j$th BS as

$$\tilde{\alpha}_j^m = \arg\min_{\forall\tilde{\alpha}_j} \mathcal{C}_L(\tilde{\alpha}_j), \quad \forall\tilde{\alpha}_j = [0^\circ, 360^\circ). \tag{24}$$

Note that the original $\mathbf{H}$ matrix in (16) for the computation of $\mathcal{C}_L$ cannot be obtained owing to the required true MS's position and noiseless relative distances. The estimated matrix $\hat{\mathbf{H}}$ can be calculated based on the initial estimate $\hat{\boldsymbol{x}}^o$ and the measurement distance $\boldsymbol{r}$ as

$$\begin{aligned} \hat{\mathbf{H}} &= \begin{bmatrix} \frac{x_1 - \hat{x}^o}{r_1} & \cdots & \frac{x_i - \hat{x}^o}{r_i} & \cdots & \frac{\tilde{x}_j - \hat{x}^o}{r_j} & \cdots & \frac{x_N - \hat{x}^o}{r_N} \\ \frac{y_1 - \hat{y}^o}{r_1} & \cdots & \frac{y_i - \hat{y}^o}{r_i} & \cdots & \frac{\tilde{y}_j - \hat{y}^o}{r_j} & \cdots & \frac{y_N - \hat{y}^o}{r_N} \\ \frac{1}{2r_1} & \cdots & \frac{1}{2r_i} & \cdots & \frac{1}{2r_j} & \cdots & \frac{1}{2r_N} \end{bmatrix} \\ &= \begin{bmatrix} \cos\hat{\alpha}_1 & \cdots & \cos\hat{\alpha}_i & \cdots & \cos\tilde{\alpha}_j & \cdots & \cos\hat{\alpha}_N \\ \sin\hat{\alpha}_1 & \cdots & \sin\hat{\alpha}_i & \cdots & \sin\tilde{\alpha}_j & \cdots & \sin\hat{\alpha}_N \\ \frac{1}{2r_1} & \cdots & \frac{1}{2r_i} & \cdots & \frac{1}{2r_j} & \cdots & \frac{1}{2r_N} \end{bmatrix}, \end{aligned} \tag{25}$$

where $\hat{\alpha}_i$ in (25) represents the $i$th BS's estimated orientation based on the initial estimate $\hat{\boldsymbol{x}}^o$. The parameters $\tilde{\boldsymbol{x}}_j = (\tilde{x}_j, \tilde{y}_j)$ and $\tilde{\alpha}_j$ in (25) denote the position and orientation of the $j$th fictitiously moveable BS, respectively. It is noticed that the design of proposed GAL scheme also considers the effect coming from the approximation of matrix $\hat{\mathbf{H}}$. As shown in Fig. 3b, the orientation of the fictitiously moved BS is considered to center at the MS's estimated position instead of the true MS's position as in Fig. 3a. It can be observed that the selection of fictitiously moveable BS may induce additional error since it is designed based on the imperfect initial estimate even though it can provide better geometry for location estimation. This demonstrates the

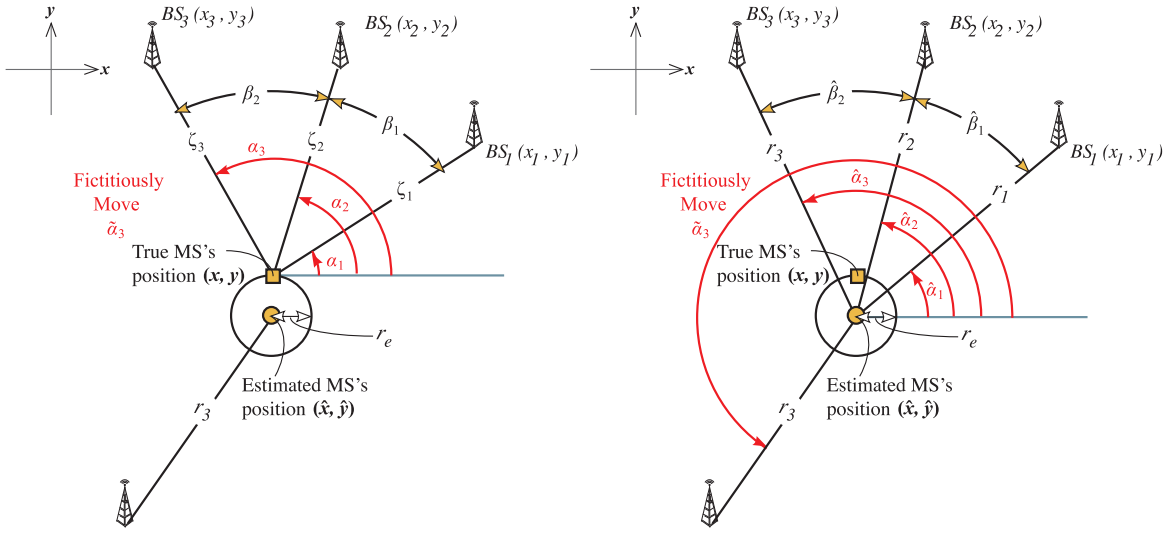


(a) An example of one fictitiously movable BS centered at the true MS's position.

(b) An example of one fictitiously movable BS centered at the estimated MS's position.

Fig. 3. Schematic diagrams of GAL with one fictitiously movable BS scheme.

situation that the fictitiously moveable BS may not always result in lowered L-CRLB value than the original network layout as stated in the constraint of problem (23). Note that the initial estimation error can be approximated as a Gaussian noise distribution with the standard deviation of the initial estimation error $\sigma_{r_e}$, i.e., $\mathcal{N}(0, \sigma_{r_e}^2)$ where $\sigma_{r_e}$ depends on the precision of the initial estimate $\hat{\boldsymbol{x}}^o$. Providing that the LLS-based estimation is used for the initial estimation, the matrix $\mathbf{I}_\zeta$ for the computation of $\mathcal{C}_L$ can be derived based on the precision of MS's initial estimate $\sigma_{r_e}$ as $\mathbf{I}_\zeta = \text{diag}\{[\sigma_{r_1}^{-2}, \ldots, \sigma_{r_i}^{-2}, \ldots, (\sigma_{r_j}^2 + \sigma_{r_e}^2)^{-1}, \ldots, \sigma_{r_N}^{-2}]\}$. The L-CRLB $\mathcal{C}_L(\tilde{\alpha}_j)$ in (24) can thus be derived as

$$\begin{aligned}\mathcal{C}_L(\tilde{\alpha}_j) = \frac{1}{D_\theta}\Bigg[&\left(\sum_{\substack{i=1\\(i\neq j)}}^{N}\frac{\sin\hat{\alpha}_i}{2\sigma_{r_i}^2\cdot r_i} + \frac{\sin\tilde{\alpha}_j}{2(\sigma_{r_j}^2+\sigma_{r_e}^2)\cdot r_j}\right)^2 \\ &+ \left(\sum_{\substack{i=1\\(i\neq j)}}^{N}\frac{\cos\hat{\alpha}_i}{2\sigma_{r_i}^2\cdot r_i} + \frac{\cos\tilde{\alpha}_j}{2(\sigma_{r_j}^2+\sigma_{r_e}^2)\cdot r_j}\right)^2 \\ &+ \sum_{\substack{i=1\\(i\neq j)}}^{N}\frac{N}{4\sigma_{r_i}^2\cdot r_i^2} + \frac{N}{4(\sigma_{r_j}^2+\sigma_{r_e}^2)\cdot r_j^2}\Bigg],\end{aligned} \tag{26}$$

where $D_\theta$ denotes for the determinant of FIM matrix $\mathbf{I}_{\boldsymbol{\theta}}$. By neglecting the terms in (26) that are not related to the parameter $\tilde{\alpha}_j$, the *equivalent one fictitiously movable BS problem* as presented in problem (24) can be obtained as

$$\begin{aligned}\tilde{\alpha}_j^m &= \arg\min_{\forall\tilde{\alpha}_j} f_1(\tilde{\alpha}_j) \\ &= \arg\min_{\forall\tilde{\alpha}_j}\frac{1}{D_\theta}\Bigg[\left(\sum_{\substack{i=1\\(i\neq j)}}^{N}\frac{\sin\hat{\alpha}_i}{2\sigma_{r_i}^2\cdot r_i} + \frac{\sin\tilde{\alpha}_j}{2(\sigma_{r_j}^2+\sigma_{r_e}^2)\cdot r_j}\right)^2 \\ &\quad + \left(\sum_{\substack{i=1\\(i\neq j)}}^{N}\frac{\cos\hat{\alpha}_i}{2\sigma_{r_i}^2\cdot r_i} + \frac{\cos\tilde{\alpha}_j}{2(\sigma_{r_j}^2+\sigma_{r_e}^2)\cdot r_j}\right)^2\Bigg],\end{aligned} \tag{27}$$

where $f_1(\tilde{\alpha}_j)$ can be regarded as the cost function of the considered problem. It can be observed that the solution of problem (27) can be acquired if the following conditions on the first and second derivatives of $f_1(\tilde{\alpha}_j)$ are satisfied, i.e.,

$$\left[\frac{\partial f_1(\tilde{\alpha}_j)}{\partial\tilde{\alpha}_j}\right]_{\tilde{\alpha}_j=\tilde{\alpha}_j^m} = 0, \tag{28}$$

$$\left[\frac{\partial^2 f_1(\tilde{\alpha}_j)}{\partial^2\tilde{\alpha}_j}\right]_{\tilde{\alpha}_j=\tilde{\alpha}_j^m} > 0. \tag{29}$$

Due to the complex formulation of (27)-(29), there does not exist closed form for obtaining the optimal value of $\tilde{\alpha}_j^m$. In order to solve the optimum rotated angle $\tilde{\alpha}_j^m$, root-finding algorithms can be utilized to find suitable solution candidates between $[0, 360^\circ)$ in (28), and these solutions will further be examined to satisfy the requirement of (29). If there are still multiple candidates that fits all the requirements, i.e., there are multiple local minimums for problem (24), the angle $\tilde{\alpha}_j^m$ that possesses with the global minimum L-CRLB value will be chosen from (26) among those solution candidates.

Furthermore, in order to reduce the computation complexity, a cost function $g_1(\tilde{\alpha}_j)$ is defined to simplify the original problem (24) without the consideration of $D_\theta$ in (27). An *approximate one fictitiously movable BS problem* can, therefore, be obtained as

$$\begin{aligned}\tilde{\alpha}_j^m &= \arg\min_{\forall\tilde{\alpha}_j} g_1(\tilde{\alpha}_j) \\ &= \arg\min_{\forall\tilde{\alpha}_j}\Bigg[\left(\sum_{\substack{i=1\\(i\neq j)}}^{N}\frac{\sin\hat{\alpha}_i}{2\sigma_{r_i}^2\cdot r_i} + \frac{\sin\tilde{\alpha}_j}{2(\sigma_{r_j}^2+\sigma_{r_e}^2)\cdot r_j}\right)^2 \\ &\quad + \left(\sum_{\substack{i=1\\(i\neq j)}}^{N}\frac{\cos\hat{\alpha}_i}{2\sigma_{r_i}^2\cdot r_i} + \frac{\cos\tilde{\alpha}_j}{2(\sigma_{r_j}^2+\sigma_{r_e}^2)\cdot r_j}\right)^2\Bigg].\end{aligned} \tag{30}$$

It is interesting to notice that the cost function $g_1(\tilde{\alpha}_j)$ can be closely related to the conditions stated in (19) for Corollary 1. Providing that the minimum value of $g_1(\tilde{\alpha}_j)$

approaches zero, the two conditions in (19) can be satisfied by solving problem (30). In other words, by fictitiously moving the $j$th BS via angle $\tilde{\alpha}_j^m$ with the consideration of $\sigma_{r_e}$ for initial estimate, the layout with the smallest linearization loss can possibly be achieved where the L-CRLB is equivalent to the CRLB. Therefore, based on the design of fictitious movable BS, the two square terms within $g_1(\tilde{\alpha}_j)$ can be treated as the extension of the two error terms $\varepsilon_1$ and $\varepsilon_2$ as described after Corollary 1 that affect the precision of linearized location estimators. By considering the first derivative of $g_1(\tilde{\alpha}_j)$ equal to zero, the rotated angle $\tilde{\alpha}_j^m$ for this problem can be derived as

$$\tilde{\alpha}_j^m = \tan^{-1}\left(\sum_{\substack{i=1\\(i\neq j)}}^{N}\frac{\cos\hat{\alpha}_i}{2\sigma_{r_i}^2\cdot r_i}\right)\Bigg/\left(\sum_{\substack{i=1\\(i\neq j)}}^{N}\frac{\sin\hat{\alpha}_i}{2\sigma_{r_i}^2\cdot r_i}\right). \tag{31}$$

Note that the angle $\tilde{\alpha}_j^m$ does not depend on any information from the $j$th BS, i.e., the measurement of the $j$th BS. The angle $\tilde{\alpha}_j^m$ lies in the domain of arc tangent function between $(-90^\circ, 90^\circ)$ which is half of the domain of $[0, 360^\circ)$. Since both angles $\tilde{\alpha}_j^m$ and $\tilde{\alpha}_j^m + 180^\circ$ can be the local minimum of the subproblem (30), these two angles will be further substituted into (26) to choose the angle with smaller L-CRLB value.

Following the procedures as stated above, all the BSs can be fictitiously moved and the associated rotated angle $\tilde{\alpha}_j^m$ can be obtained. The $j^m$th BS with the minimum L-CRLB value will be selected to be the fictitiously moveable BS for the GAL(1BS) scheme in problem (23). For example as shown in Fig. 3, only the third BS, i.e., $j^m = 3$, is fictitiously adjusted and the other two BSs remain at the same position. The $j^m$th fictitiously moved BS will be relocated to the coordinate as

$$\begin{cases}\tilde{x}_{j^m} = r_{j^m}\cos(\tilde{\alpha}_j^m),\\ \tilde{y}_{j^m} = r_{j^m}\sin(\tilde{\alpha}_j^m).\end{cases} \tag{32}$$

Note that the measurement of the $j^m$th BS remains the same as $r_{j^m}$. The noise variance of this measurement is recalculated as $\sigma_{r_j}^2 + \sigma_{r_e}^2$. Based on the new set of BSs adjusted by the proposed GAL(1BS) scheme, the LLS-based estimation can be adopted to obtain the final estimation of MS's position.

### 3.2 GAL with Two Fictitiously Movable BSs Scheme

The GAL(2BSs) scheme is designed to fictitiously relocate the position of two BSs according to the minimal L-CRLB layout criterion. Under this condition, two BSs are defined to be fictitiously movable and the others are fixed. The objective of the GAL(2BSs) scheme is to select the specific two BSs that should be fictitiously moved in order to achieve the layout with the minimum L-CRLB. The *GAL(2BSs) problem* is defined as

$$\begin{aligned}\{j^m, k^m\} = \arg\min_{j=1,\ldots,N,k=1,\ldots,N,j\neq k} \quad & \mathcal{C}_L(\tilde{\alpha}_j^m, \tilde{\alpha}_k^m)\\ \text{subject to} \quad & \mathcal{C}_L(\tilde{\alpha}_j^m, \tilde{\alpha}_k^m) < \mathcal{C}_L,\end{aligned} \tag{33}$$

where $\tilde{\alpha}_j^m$ and $\tilde{\alpha}_k^m$ represent the orientation of two fictitiously moveable BSs. The constraint in (33) is to verify if the original L-CRLB has already been the lowest under the given measurement conditions. Before solving problem (33), the optimum rotated angles $\tilde{\alpha}_j^m$ and $\tilde{\alpha}_k^m$ of the two fictitiously movable BSs should be decided first. The *two fictitiously movable BSs problem* is defined to find the optimum rotated angles as

$$\{\tilde{\alpha}_j^m, \tilde{\alpha}_k^m\} = \arg\min_{\forall\tilde{\alpha}_j,\tilde{\alpha}_k, j\neq k} \mathcal{C}_L(\tilde{\alpha}_j, \tilde{\alpha}_k), \forall\tilde{\alpha}_j, \tilde{\alpha}_k = [0^\circ, 360^\circ). \tag{34}$$

Note that the matrix $\mathbf{I}_{\boldsymbol{\zeta}}$ in $\mathcal{C}_L(\tilde{\alpha}_j, \tilde{\alpha}_k)$ can be obtained as $\mathbf{I}_{\boldsymbol{\zeta}} = \mathrm{diag}\{[\sigma_{r_1}^{-2}, \ldots, (\sigma_{r_j}^2 + \sigma_{r_e}^2)^{-1}, \ldots, (\sigma_{r_k}^2 + \sigma_{r_e}^2)^{-1}, \ldots, \sigma_{r_N}^{-2}]\}$, where the standard deviation $\sigma_{r_e}$ of MS's initial estimate is considered in both the $j$th and $k$th fictitiously movable BSs. Therefore, the L-CRLB can be derived as

$$\begin{aligned}&\mathcal{C}_L(\tilde{\alpha}_j, \tilde{\alpha}_k) =\\ &\frac{1}{D_\theta}\Bigg[\left(\sum_{\substack{i=1\\(i\neq j,k)}}^{N}\frac{\sin\hat{\alpha}_i}{2\sigma_{r_i}^2\cdot r_i} + \frac{\sin\tilde{\alpha}_j}{2(\sigma_{r_j}^2+\sigma_{r_e}^2)\cdot r_j} + \frac{\sin\tilde{\alpha}_k}{2(\sigma_{r_k}^2+\sigma_{r_e}^2)\cdot r_k}\right)^2\\ &+\left(\sum_{\substack{i=1\\(i\neq j,k)}}^{N}\frac{\cos\hat{\alpha}_i}{2\sigma_{r_i}^2\cdot r_i} + \frac{\cos\tilde{\alpha}_j}{2(\sigma_{r_j}^2+\sigma_{r_e}^2)\cdot r_j} + \frac{\cos\tilde{\alpha}_k}{2(\sigma_{r_k}^2+\sigma_{r_e}^2)\cdot r_k}\right)^2\\ &+\sum_{\substack{i=1\\(i\neq j,k)}}^{N}\frac{N}{4\sigma_{r_i}^2\cdot r_i^2} + \frac{N}{4(\sigma_{r_j}^2+\sigma_{r_e}^2)\cdot r_j^2} + \frac{N}{4(\sigma_{r_k}^2+\sigma_{r_e}^2)\cdot r_k^2}\Bigg].\end{aligned} \tag{35}$$

Similar to the GAL(1BS) scheme, the *equivalent two fictitiously movable BSs problem* for problem (34) can also be acquired as

$$\{\tilde{\alpha}_j^m, \tilde{\alpha}_k^m\} = \arg\min_{\forall\tilde{\alpha}_j,\tilde{\alpha}_k, j\neq k} f_2(\tilde{\alpha}_j, \tilde{\alpha}_k), \tag{36}$$

where $f_2(\tilde{\alpha}_j, \tilde{\alpha}_k)$ is regarded as the cost function of problem (36) as

$$\begin{aligned}&f_2(\tilde{\alpha}_j, \tilde{\alpha}_k) =\\ &\frac{1}{D_\theta}\Bigg[\left(\sum_{\substack{i=1\\(i\neq j,k)}}^{N}\frac{\sin\hat{\alpha}_i}{2\sigma_{r_i}^2\cdot r_i} + \frac{\sin\tilde{\alpha}_j}{2(\sigma_{r_j}^2+\sigma_{r_e}^2)\cdot r_j} + \frac{\sin\tilde{\alpha}_k}{2(\sigma_{r_k}^2+\sigma_{r_e}^2)\cdot r_k}\right)^2\\ &+\left(\sum_{\substack{i=1\\(i\neq j,k)}}^{N}\frac{\cos\hat{\alpha}_i}{2\sigma_{r_i}^2\cdot r_i} + \frac{\cos\tilde{\alpha}_j}{2(\sigma_{r_j}^2+\sigma_{r_e}^2)\cdot r_j} + \frac{\cos\tilde{\alpha}_k}{2(\sigma_{r_k}^2+\sigma_{r_e}^2)\cdot r_k}\right)^2\Bigg].\end{aligned} \tag{37}$$

It can be observed that problem (36) can be solved if the following conditions on the first derivatives of $f_2(\tilde{\alpha}_j, \tilde{\alpha}_k)$ are satisfied, i.e.,

$$\left[\frac{\partial f_2(\tilde{\alpha}_j, \tilde{\alpha}_k)}{\partial\tilde{\alpha}_j}\right]_{\substack{\tilde{\alpha}_j=\tilde{\alpha}_j^m\\ \tilde{\alpha}_k=\tilde{\alpha}_k^m}} = 0, \left[\frac{\partial f_2(\tilde{\alpha}_j, \tilde{\alpha}_k)}{\partial\tilde{\alpha}_k}\right]_{\substack{\tilde{\alpha}_j=\tilde{\alpha}_j^m\\ \tilde{\alpha}_k=\tilde{\alpha}_k^m}} = 0, \tag{38}$$

and the conditions on the second derivatives of $f_2(\tilde{\alpha}_j, \tilde{\alpha}_k)$ are also fulfilled, i.e., $a > 0$ and $ac - b^2 > 0$, where

$$\begin{aligned}a &= \left[\frac{\partial^2 f_2(\tilde{\alpha}_j, \tilde{\alpha}_k)}{\partial^2\tilde{\alpha}_j}\right]_{\substack{\tilde{\alpha}_j=\tilde{\alpha}_j^m\\ \tilde{\alpha}_k=\tilde{\alpha}_k^m}}, b = \left[\frac{\partial^2 f_2(\tilde{\alpha}_j, \tilde{\alpha}_k)}{\partial\tilde{\alpha}_j\partial\tilde{\alpha}_k}\right]_{\substack{\tilde{\alpha}_j=\tilde{\alpha}_j^m\\ \tilde{\alpha}_k=\tilde{\alpha}_k^m}},\\ c &= \left[\frac{\partial^2 f_2(\tilde{\alpha}_j, \tilde{\alpha}_k)}{\partial^2\tilde{\alpha}_k}\right]_{\substack{\tilde{\alpha}_j=\tilde{\alpha}_j^m\\ \tilde{\alpha}_k=\tilde{\alpha}_k^m}},\end{aligned} \tag{39}$$

Since the closed form solution of $\tilde{\alpha}_j^m$ and $\tilde{\alpha}_k^m$ can not be obtained in this case, numerical methods can be used to

acquire the optimal angles $\tilde{\alpha}_j^m$ and $\tilde{\alpha}_k^m$ for achieving minimum L-CRLB for problem (36). To reduce the computation complexity, a cost function $g_2(\tilde{\alpha}_j, \tilde{\alpha}_k)$ is defined to simplify the original problem (34) into an *approximate two fictitiously movable BSs problem*

$$\{\tilde{\alpha}_j^m, \tilde{\alpha}_k^m\} = \arg \min_{\forall \tilde{\alpha}_j, \tilde{\alpha}_k, j \neq k} g_2(\tilde{\alpha}_j, \tilde{\alpha}_k), \tag{40}$$

where

$$g_2(\tilde{\alpha}_j, \tilde{\alpha}_k) = \left( \sum_{\substack{i=1 \\ (i \neq j,k)}}^{N} \frac{\sin \hat{\alpha}_i}{2\sigma_{r_i}^2 \cdot r_i} + \frac{\sin \tilde{\alpha}_j}{2(\sigma_{r_j}^2 + \sigma_{r_e}^2) \cdot r_j} + \frac{\sin \tilde{\alpha}_k}{2(\sigma_{r_k}^2 + \sigma_{r_e}^2) \cdot r_k} \right)^2 + \left( \sum_{\substack{i=1 \\ (i \neq j,k)}}^{N} \frac{\cos \hat{\alpha}_i}{2\sigma_{r_i}^2 \cdot r_i} + \frac{\cos \tilde{\alpha}_j}{2(\sigma_{r_j}^2 + \sigma_{r_e}^2) \cdot r_j} + \frac{\cos \tilde{\alpha}_k}{2(\sigma_{r_k}^2 + \sigma_{r_e}^2) \cdot r_k} \right)^2, \tag{41}$$

The closed form solution of (40) for the $N = 3$ case is illustrated as follows: For ease of computation, the three BSs' orientation can be represented by their adjacent included angles as $\hat{\boldsymbol{\alpha}} = \{\hat{\alpha}_1 = \hat{\alpha}_2 - \hat{\beta}_1, \hat{\alpha}_2, \hat{\alpha}_3 = \hat{\alpha}_2 + \hat{\beta}_2\}$ as shown in Fig. 3. The GAL(2BSs) scheme fictitiously relocates the positions of two BSs among the three which can be denoted as $\tilde{\boldsymbol{\alpha}} = \{\hat{\alpha}_2 - \tilde{\beta}_1, \hat{\alpha}_2, \hat{\alpha}_2 - \tilde{\beta}_2\}$. Furthermore, according to the rotation property, the orientation of the fictitiously moved BSs can be transformed as $\tilde{\boldsymbol{\alpha}} = \{-\tilde{\beta}_1, 0^\circ, -\tilde{\beta}_2\}$. By considering the first derivative equation in (38), the BSs' adjacent included angles for achieving the minimum CRLB are calculated as

$$\begin{aligned} \tilde{\beta}_1^m = \cos^{-1} \{ & [(\sigma_{r_1}^2 + \sigma_{r_e}^2)^2 r_1^2 \sigma_{r_2}^4 r_2^2 \\ & - \sigma_{r_2}^4 r_2^2 (\sigma_{r_3}^2 + \sigma_{r_e}^2)^2 r_3^2 - (\sigma_{r_1}^2 + \sigma_{r_e}^2)^2 r_1^2 (\sigma_{r_3}^2 + \sigma_{r_e}^2)^2 r_3^2 ] / \\ & [2(\sigma_{r_1}^2 + \sigma_{r_e}^2) r_1 \cdot \sigma_{r_2}^2 r_2 \cdot (\sigma_{r_3}^2 + \sigma_{r_e}^2)^2 r_3^2] \}, \end{aligned} \tag{42}$$

$$\begin{aligned} \tilde{\beta}_2^m = \cos^{-1} \{ & [\sigma_{r_2}^4 r_2^2 (\sigma_{r_3}^2 + \sigma_{r_e}^2)^2 r_3^2 \\ & - (\sigma_{r_1}^2 + \sigma_{r_e}^2)^2 r_1^2 (\sigma_{r_3}^2 + \sigma_{r_e}^2)^2 r_3^2 - (\sigma_{r_1}^2 + \sigma_{r_e}^2)^2 r_1^2 \sigma_{r_2}^4 r_2^2 ] / \\ & [2(\sigma_{r_1}^2 + \sigma_{r_e}^2)^2 r_1^2 \cdot \sigma_{r_2}^2 r_2 \cdot (\sigma_{r_3}^2 + \sigma_{r_e}^2) r_3] \}, \end{aligned} \tag{43}$$

where the angle $\tilde{\beta}_j^m$ for $j = 1$ and 2 lies in the domain of arc cosine function from $[0, 180^\circ]$ which is half of the domain $[0, 360^\circ)$. Both angles $\tilde{\beta}_j^m$ and $\tilde{\beta}_j^m + 180^\circ$ are considered the local minimums of subproblem (40). Therefore, these angles will be substituted into (35) to determine the angle with smaller L-CRLB value. After the adjacent included angles are calculated, the BSs' orientation of the GAL(2BSs) scheme can be acquired as $\tilde{\boldsymbol{\alpha}}^m = \{\tilde{\alpha}_1^m = \hat{\alpha}_2 - \tilde{\beta}_1^m, \hat{\alpha}_2, \tilde{\alpha}_3^m = \hat{\alpha}_2 + \tilde{\beta}_2^m\}$. Accordingly, all the BSs can be fictitiously moved and the associated rotated angle $\tilde{\alpha}_j^m$ and $\tilde{\alpha}_k^m$ will be obtained. The $j^m$th and $k^m$th BSs with the minimum L-CRLB value are decided to be the fictitiously moveable BS for the GAL(2BSs) scheme in problem (33). The positions of $j^m$th and $k^m$th BSs can be fictitiously relocated and computed based on (32). Note that the measurement remains the same while the noise variance of the measurement is recalculated by considering the initial estimation error. With the new set of BSs obtained from the GAL(2BSs) scheme, the LLS-based estimation algorithms can be adopted to obtain the final MS's location estimation. Based on the derivation of proposed GAL(2BSs) scheme, the number of fictitiously movable BSs can also be increased by extending the GAL scheme with multivariable optimization, i.e., GAL(3BSs), GAL(4BSs).

### 3.3 GAL Scheme

Based on Sections 3.1 and 3.2, it can be observed that the GAL(2BSs) scheme provides one more degree of freedom compared to the GAL(1BS) scheme, which should increase the precision of location estimation owing to the enhancement from the geometric effect. However, the two fictitiously moveable BSs associate with the initial MS's estimation error may degrade the performance for location estimation. Therefore, the GAL scheme for the $N = 3$ case is designed to select between the two sub-schemes, i.e., GAL(1BS) and GAL(2BSs), in order to achieve minimum L-CRLB value among all different cases. The *GAL problem* can be defined as

$$\begin{aligned} \tilde{\boldsymbol{\alpha}}^m = \arg \min_{\tilde{\boldsymbol{\alpha}}_{1BS}^m, \tilde{\boldsymbol{\alpha}}_{2BS}^m} \quad & [\mathcal{C}_L(\tilde{\boldsymbol{\alpha}}_{1BS}^m), \mathcal{C}_L(\tilde{\boldsymbol{\alpha}}_{2BS}^m)] \\ \text{subject to} \quad & \mathcal{C}_L(\tilde{\boldsymbol{\alpha}}_{1BS}^m), \mathcal{C}_L(\tilde{\boldsymbol{\alpha}}_{2BS}^m) < \mathcal{C}_L, \end{aligned} \tag{44}$$

where $\tilde{\boldsymbol{\alpha}}_{1BS}^m$ and $\tilde{\boldsymbol{\alpha}}_{2BS}^m$ represent the sets of BS's orientation with the lowest L-CRLB by adopting the GAL(1BS) and GAL(2BSs) schemes, respectively. Each of the fictitiously moved BS set is selected according to the minimum L-CRLB criteria. Note that if both the GAL(1BS) and GAL(2BSs) schemes cannot provide a lower L-CRLB scenario compared to the original unmoved version, the GAL scheme will choose the original BS's positions for MS's location estimation according to the constraint in (44).

## 4 Implementations of Proposed Geometry-Assisted Localization Algorithm

As described in previous section, the main objective of the proposed GAL scheme is to acquire the positions of fictitiously movable BSs in order to provide better geometric layout for MS's location estimation. Since the GAL scheme is designed based on the initial estimate of the MS, there can be different implementations to adopt the GAL scheme for location estimation. Fig. 4 illustrates the schematic diagrams for the implementations of the proposed GAL algorithm. The GAL-TSLS scheme as shown in Fig. 4a is proposed to calculate both the initial and final estimates of the MS's position based on the two-step LS estimator [9]. On the other hand, a two-stage architecture named GAL-KF scheme as shown in Fig. 4b, i.e., a two-step LS estimator with a Kalman filter, is proposed to enhance the initial estimate with the historical information from Kalman filter. These two types of implementations of GAL scheme are explained in the following two sections.

### 4.1 GAL with Two-Step LS Estimator

As shown in Fig. 4a, the MS's initial estimate $\hat{\boldsymbol{x}}^o$ can be obtained by performing the two-step LS method. The concept of the two-step LS method is to acquire an intermediate location estimate in the first step by assuming that $\boldsymbol{x}$ and $R$ are not correlated. Note that this first step is

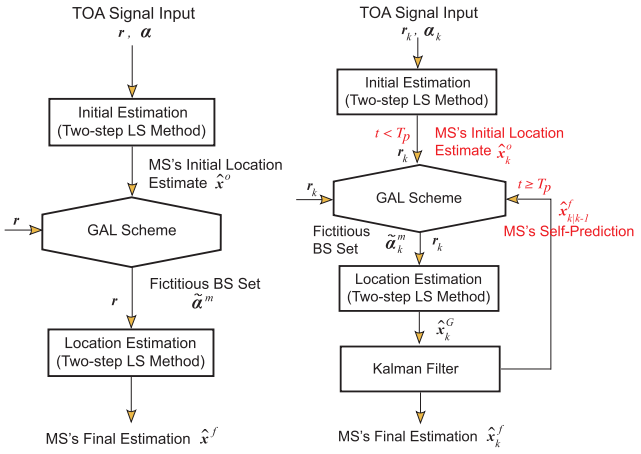


(a) Proposed GAL-TSLS scheme. (b) Proposed GAL-KF scheme.

Fig. 4. Implementations of proposed GAL algorithm.

exactly the LLS method [5] which solves the L-LEP instead of the conventional LEP. By combining (1) and (2), the elements within the matrix formulation (i.e., $\mathbf{M}_1\boldsymbol{\theta} = \mathbf{J}_1$) for the first step of the estimator can be obtained as

$$\mathbf{M}_1 = \begin{bmatrix} -2x_1 & -2y_1 & 1 \\ -2x_2 & -2y_2 & 1 \\ . & . & . \\ -2x_N & -2y_N & 1 \end{bmatrix} \quad \mathbf{J}_1 = \begin{bmatrix} r_1^2 - \kappa_1 \\ r_2^2 - \kappa_2 \\ . \\ r_N^2 - \kappa_N \end{bmatrix},$$

where $\kappa_i = x_i^2 + y_i^2$. The parameter set $\hat{\boldsymbol{\theta}} = [x^{(1)}\ y^{(1)}\ R^{(1)}]^T$ that is to be estimated at the first step can be acquired as

$$\hat{\boldsymbol{\theta}} = \left(\mathbf{M}_1^T \boldsymbol{\Psi}_1^{-1} \mathbf{M}_1\right)^{-1} \mathbf{M}_1^T \boldsymbol{\Psi}_1^{-1} \mathbf{J}_1. \tag{45}$$

The error of the first step estimation is obtained as $\psi_1 = \mathbf{M}_1\hat{\boldsymbol{\theta}} - \mathbf{J}_1 = 2\mathbf{B}_1\mathbf{n}_1 + \mathbf{n}_1^2$ where $\mathbf{n}_1 = [n_1, \ldots, n_i, \ldots, n_N]^T$ represents the measurement noise vector in (1). Therefore, the weighting matrix $\boldsymbol{\Psi}_1$ in (45) can be acquired by neglecting the square term $\mathbf{n}_1^2$ as

$$\boldsymbol{\Psi}_1 = E[\psi_1\psi_1^T] = 4\mathbf{B}_1\, E\left[\mathbf{n}_1\mathbf{n}_1^T\right] \mathbf{B}_1 = 4\mathbf{B}_1\mathbf{I}_\zeta\mathbf{B}_1, \tag{46}$$

where $\mathbf{B}_1 = \mathrm{diag}\{[r_1, \ldots, r_i, \ldots, r_N]\}$. The second step of the two-step LS method releases this assumption that $\boldsymbol{x}$ and $R$ are uncorrelated by adjusting the intermediate result to obtain an improved location estimate. Therefore, the correlation relationship can be applied and the elements within the second step of the two-step LS estimator formulation, i.e., $\mathbf{M}_2\hat{\boldsymbol{x}}^{(2)} = \mathbf{J}_2$, are obtained as

$$\mathbf{M}_2 = \begin{bmatrix} 1 & 0 & 0 \\ 0 & 1 & 0 \\ 1 & 1 & 0 \end{bmatrix} \quad \mathbf{J}_2 = \begin{bmatrix} (x^{(1)})^2 \\ (y^{(1)})^2 \\ R^{(1)} \end{bmatrix}, \tag{47}$$

with $\hat{\boldsymbol{x}}^{(2)} = [(x^{(2)})^2, (y^{(2)})^2]^T$. It can also be solved by the weighted LS formulation with the weighting matrix $\boldsymbol{\Psi}_2$ of the second step as

$$\boldsymbol{\Psi}_2 = 4\mathbf{B}_2\mathrm{cov}(\hat{\boldsymbol{\theta}})\mathbf{B}_2 = 4\mathbf{B}_2\left(\mathbf{M}_1{}^T\boldsymbol{\Psi}_1{}^{-1}\mathbf{M}_1\right)^{-1}\mathbf{B}_2, \tag{48}$$

where $\mathbf{B}_2 = \mathrm{diag}\{[x^{(1)}, y^{(1)}, 1/2]\}$. With the relationship of $R = x^2 + y^2$, it can be observed that the variable $R$ is removed from $\hat{\boldsymbol{\theta}}$ such as to form the reduced dimension vector of $\boldsymbol{x}^{(2)}$. The MS's position estimate by using the two-step LS estimator can be obtained by taking element-wise square root as $\hat{\boldsymbol{x}} = (\hat{\boldsymbol{x}}^{(2)})^{1/2} = [x^{(2)}, y^{(2)}]^T$.

As shown in Fig. 4a, the two-step LS estimator is performed to obtain an initial estimate $\hat{\boldsymbol{x}}^o$. With the initial estimate, the fictitious BS set can be calculated based on the proposed GAL scheme targeting on achieving the minimum L-CRLB requirement. The two-step LS is performed for the second time with the adjusted BSs and the received measurements to obtain the MS's location estimate for the GAL-TSLS scheme.

### 4.2 GAL with Kalman Filter

In order to provide enhanced location estimate, the proposed GAL-KF scheme as shown in Fig. 4b is suggested to estimate the MS's position using a two-stage estimator, i.e., a two-step LS estimator with a Kalman filter. The Kalman filtering technique is employed to estimate the MS's position based on its previously estimated data. The measurement and state equations at the $k$th time step for the Kalman filter can be represented as

$$\mathbf{z}_k = \mathbf{E}\hat{\boldsymbol{x}}_k^f + \mathbf{m}_k, \tag{49}$$

$$\hat{\boldsymbol{x}}_k^f = \mathbf{F}\hat{\boldsymbol{x}}_{k-1}^f + \mathbf{p}_k, \tag{50}$$

where $\hat{\boldsymbol{x}}_k^f$ represents the output and $\mathbf{z}_k$ denotes the measurement input of the Kalman filter. Note that for the two-stage location estimation, the input of the Kalman filter is obtained from the result of the GAL scheme as $\mathbf{z}_k = \hat{\boldsymbol{x}}_k^G$ in Fig. 4b. The variables $\mathbf{m}_k$ and $\mathbf{p}_k$ denote the measurement and the process noises associated with the covariance matrices $\mathbf{R}$ and $\mathbf{Q}$ within the Kalman filtering formulation. Note that the matrix $\mathbf{R}$ can be determined by the FIM of L-CRLB and $\mathbf{Q}$ is set to be an identity matrix. Furthermore, the matrix $\mathbf{E}$ and the state transition matrix $\mathbf{F}$ in (49) and (50) respectively can be obtained as $\mathbf{E} = \mathbf{F} = \mathbf{I}_{2\times 2}$.

As shown in Fig. 4b, the execution process of the proposed GAL-KF scheme consists of two phases, including the transition period ($T_p$) and the stable period. During the transient period $t < T_p$, the GAL-KF scheme adopts the two-step LS method to provide the initial estimate of the MS. After the tracking time is longer than $T_p$, the GAL-KF scheme starts to adopt the prediction from the output of the Kalman filter, i.e., $\hat{\boldsymbol{x}}_{k|k-1}^f$, which serves as the updated initial MS's estimate for the GAL scheme. By adopting the Kalman filter, it can be observed that the GAL-KF scheme only requires to perform a single round of location estimation compared to the GAL-TSLS scheme after the system is executed in the stable state. The Kalman filter can refine the MS's position estimation with the historical measurements based on the initial estimate, which should provide better estimation accuracy by adopting the GAL-KF scheme compared to the GAL-TSLS method.

## 5 Performance Evaluation

Simulations are performed to show the effectiveness of the GAL algorithms (i.e., GAL-TSLS and GAL-KF) under different network topologies and the MS's positions. The number of BSs is considered as three in the examples since

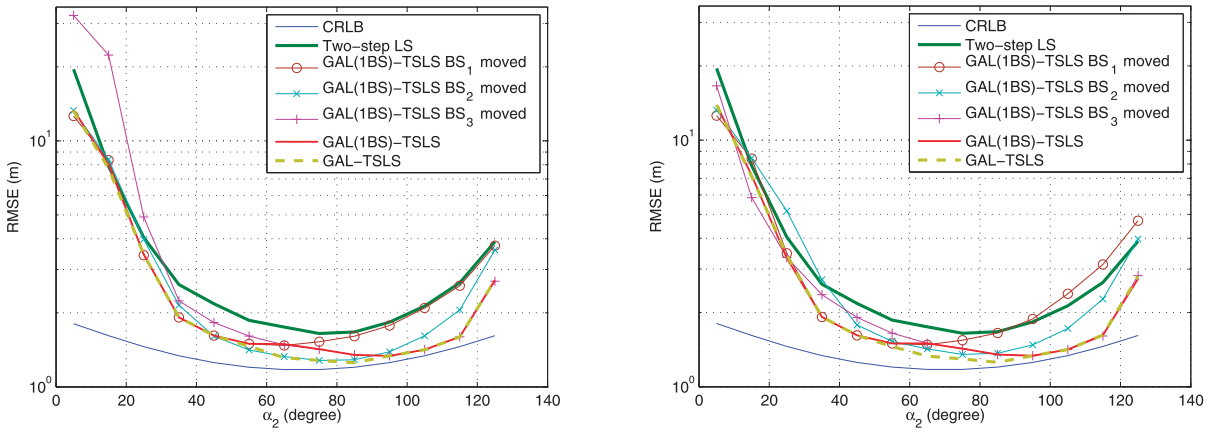


(a) GAL-TSLS with original one fictitiously movable BS problem. (b) GAL-TSLS with approximate one fictitiously movable BS problem.

Fig. 5. Validation on GAL-TSLS scheme with one fictitiously movable BS problem.

three BSs is the minimum sufficient number for the localization problem. The model for the LOS measurement noise of the TOA signals is selected as the Gaussian distribution with zero mean and standard deviation as $\sigma_n$ meters in different cases, i.e., $n_{i,k} \sim \mathcal{N}(0, \sigma_n^2)$. In the following examples 5 and 6, the GAL-TSLS algorithm is simulated to validate the effectiveness of the fictitiously movable BS schemes on the two-step LS based estimation.

**Example 5 (Validation on Approximate One Fictitiously Movable BS Problem).** The purpose of this example is to compare and validate the difference between the original and approximate one fictitiously movable BS problems. Consider an array of three sensors whose coordinates are $\boldsymbol{x}_1 = [50\cos 0°, 50\sin 0°]^T$, $\boldsymbol{x}_2 = [30\cos\alpha_2, 30\sin\alpha_2]^T$, and $\boldsymbol{x}_3 = [20\cos 140°, 20\sin 140°]^T$ where $\boldsymbol{x}_2$ is function of $\alpha_2$ with its range as indicated in the $x$-axis of Fig. 5. The MS's true position is assumed to be placed at the origin, i.e., $\boldsymbol{x} = [0, 0]^T$. Note that all the layouts formed by the three sensors with the change of $\alpha_2$ are designed to be OPLs for validation purpose. More realistic network scenarios will be considered in the following examples. The standard deviation of the Gaussian noises is chosen as $\sigma_n = 1$ in this example. The root mean square error (RMSE) is defined as

$$RMSE = \sqrt{\sum_{i=1}^{M} \|\hat{\boldsymbol{x}} - \boldsymbol{x}\|^2 / M},$$

where $M$ denotes the number of trials as 1,000. Fig. 5a shows the original one fictitiously movable BS problem obtained by exhaustively solving (24); while Fig. 5b illustrates the approximate one fictitiously movable BS problem acquired from (30) and (31), which are respectively denoted as "GAL(1BS)-TSLS $\text{BS}_i$ moved" in both plots, for $i = 1$, 2, and 3. In each of the three cases, i.e., $i = 1$, 2, and 3, $\text{BS}_i$ is fictitiously moved for obtaining the optimal angle $\tilde{\alpha}_i^m$ that can achieve the minimum value of L-CRLB. Moreover, the "GAL(1BS)-TSLS" curves in both plots respectively denote the GAL(1BS) problem as defined in (23) by selecting among different fictitiously movable angles from the original problem (24) in Fig. 5a and approximate problem (30) in Fig. 5b. Since the "GAL(1BS)-TSLS" method acquires the positions of the fictitious BSs based on the MS's initial estimate instead of the true position, the RMSE performance is not necessarily the lowest compared to the "GAL(1BS)-TSLS $\text{BS}_i$ moved" scheme for $i = 1$, 2, and 3. Both the CRLB and the conventional two-step LS scheme are also illustrated in both plots for comparison purpose.

Notice that the derived L-CRLB is to characterize the geometric property for linearized location estimation, i.e., the initial estimation of GAL algorithms. By fictitiously moving the BS locations, the GAL algorithm improves the estimation accuracy of linearized algorithm which is originally bounded by L-CRLB. In other words, the MS's location estimation error can further be reduced such that the CRLB bound will possibly be achieved. Therefore, the benchmark of localization problem should still be CRLB instead of L-CRLB. It can be observed that even though the approximate problem will be differ from the original problem by individually moving one of the three BSs fictitiously, the resulting problem (23), i.e., the GAL(1BS)-TSLS scheme, obtained from (30) will be closely match with (24) as shown in both plots. Furthermore, it can be seen that the GAL(1BS)-TSLS scheme can provide better RMSE performance compared to the conventional two-step LS scheme.

**Example 6 (Validation on Approximate Two Fictitiously Movable BSs Problem).** This example is to compare and validate the difference between the original and approximate two fictitiously movable BSs problems in Figs. 6a and 6b, respectively. Same network layout and noise variance as in example 5 are used in this example. The curves named "GAL(2BSs)-TSLS $\text{BS}_i$ fixed" refer to the problems that the $i$th BS is fixed while the other two BSs are movable, i.e., the angle set $\{\tilde{\alpha}_2^m, \tilde{\alpha}_3^m\}$ of the curve "GAL(2BSs)-TSLS $\text{BS}_1$ fixed" are obtained via (34) and (40) for the original (Fig. 6a) and approximate (Fig. 6b) problems, respectively. Moreover, the curve "GAL(2BSs)-TSLS" denotes for the problem in (33) to select among different movable angles from the original

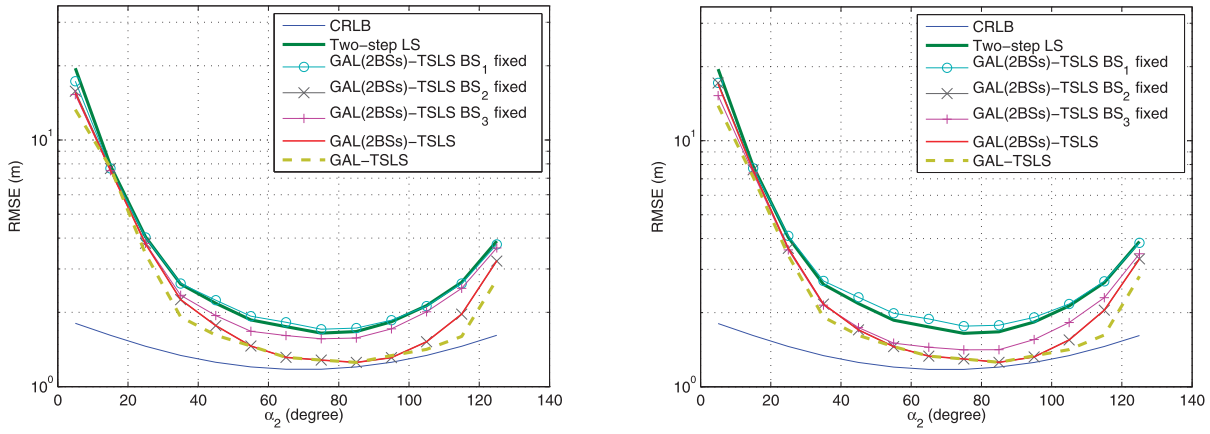


(a) GAL-TSLS with original two fictitiously movable BSs problem. (b) GAL-TSLS with approximate two fictitiously movable BSs problem.

Fig. 6. Validation on GAL-TSLS scheme with two fictitiously movable BSs problem.

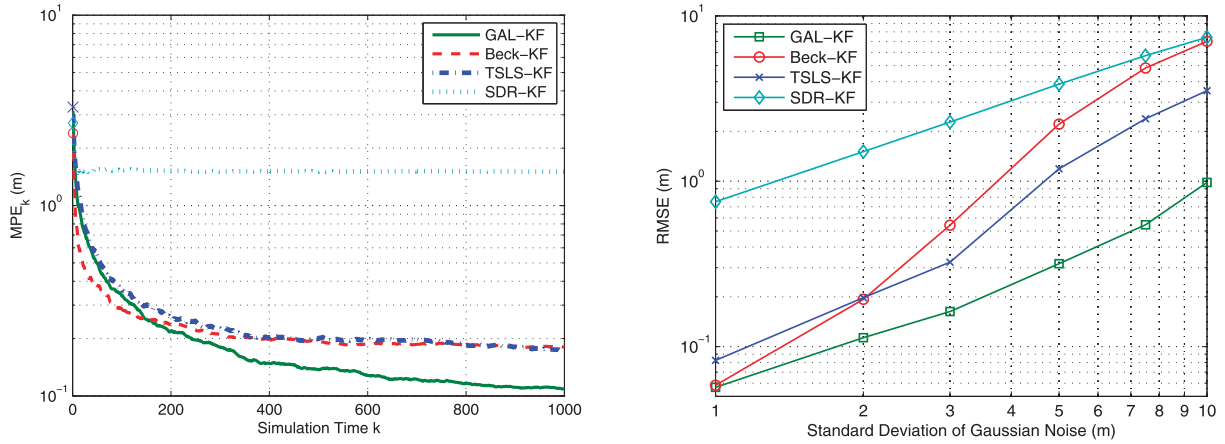


(a) MPE versus simulation time under $\sigma_n = 2$. (b) RMSE versus different $\sigma_n$.

Fig. 7. Performance comparison of example 7.

problem (34) in Fig. 6a and the approximate problem (40) in Fig. 6b. Similar to the previous example, the final GAL(2BSs)-TSLS scheme of both problems are observed to be consistent with each other from the simulation results. Meanwhile, the effectiveness of problem (44) for the GAL scheme is also validated by selecting among the GAL(1BS)-TSLS and the GAL(2BSs)-TSLS schemes. By observing both Figs. 5 and 6, the GAL-TSLS scheme with the problem (44) can achieve the lowest RMSE compared to the other methods.

It is intuitive that the closed form property of the approximate problem can provide efficiency in computational complexity compared to the original problem. Therefore, the approximate problem with the GAL scheme will be adopted in the rest of the examples for performance comparison. In order to provide better estimation precision for MS's location estimate, the GAL-KF algorithm is simulated to compare with the existing two-step LS [9], Beck [20], and SDR [21] algorithms, which are named as TSLS-KF, Beck-KF, and SDR-KF, respectively. Note that these three algorithms are also cascaded with the Kalman filters to perform two-stage estimation in order to provide fair comparison.

**Example 7 (A Special Case of GAL-KF Scheme).** In this example, a special network scenario is simulated to provide performance comparison for the GAL-KF scheme. Consider an array of three sensors in the OPL whose coordinates are $\boldsymbol{x}_1 = [20\cos 0°,\ 20\sin 0°]^T$, $\boldsymbol{x}_2 = [30\cos 80°, 30\sin 80°]^T$, and $\boldsymbol{x}_3 = [50\cos 140°, 50\sin 140°]^T$, while the MS's true position is fixed at $\boldsymbol{x} = [0,\ 0]^T$. Fig. 7a demonstrates the performance comparison of mean position error (MPE) for the simulation time interval $k = 1{,}000$, where each time instant is run with 1,000 simulation samples. Note that the MPE at the $k$th time instant is defined as $\text{MPE}_k = \sum_{i=1}^{M} \|\hat{\boldsymbol{x}}_k - \boldsymbol{x}_k\|^2/M$. The transient period $T_p$ is chosen as 20 which means that the GAL-KF scheme starts to adopt the prediction from the Kalman filter at the time instant $k = 21$. The standard deviation of Gaussian noises $\sigma_n$ is chosen as 2 in Fig. 7a. Since the Kalman filter is effective in smoothing the estimation result, it can be observed that the MPE is decreased and converges with the increment of time instant $k$ for all the schemes in Fig. 7a. With the consideration of the L-CRLB in the algorithm design, the proposed GAL-KF implementation can achieve lowered MPE compared to the other schemes; while the SDR-KF has the worst performance among all

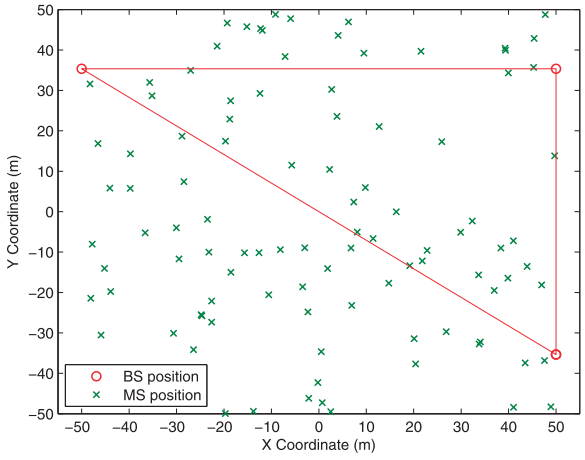


Fig. 8. Network layout of example 8.

the algorithms. Since the two-stage architecture does not provide smoothing gain to the SDR-KF method, the SDR-KF scheme will not be further considered in the rest of the simulation examples. Fig. 7b illustrates the performance comparison of RMSE at the simulation time instant $k = 1{,}000$ under different standard deviations of the Gaussian noises. It can be observed that the GAL-KF scheme can provide a significant gain over the other methods under different noise values. Note that the Beck-KF scheme is observed to be sensitive to the noise which results in higher RMSE compared to the TSLS-KF scheme under larger noise condition. For example, compared to the TSLS-KF and Beck-KF methods, the proposed GAL-KF scheme will result in 2.8 and 6 meters less of RMSE respectively under $\sigma_n = 10$ meter as shown in Fig. 7.

**Example 8 (A General Case of GAL-KF Scheme under LOS Environment).** This example illustrates a general scenario of wireless sensor network (as shown in Fig. 8) for performance comparison under LOS environment. The BSs' coordinates are selected as $\boldsymbol{x}_1 = [50,\ -35.36]^T$, $\boldsymbol{x}_2 = [50,\ 35.36]^T$, and $\boldsymbol{x}_3 = [-50,\ 35.36]^T$, and there are 100 MSs randomly deployed in a $100 \times 100$ meter square space. Note that the number of MSs located in the OPL is larger than that in the IPL in this example in order to demonstrate that the OPL may frequently occur in a sensor network environment. The performance of the IPL and the OPL under the LOS condition are separately examined under different noise standard deviation in Figs. 9a and 9b, respectively. Since the difference between the L-CRLB and the CRLB is considered small in the IPL case, similar RMSE performance is observed among the three compared schemes as illustrated in Fig. 8a. On the other hand, with the OPL scenario as shown in Fig. 8b, the GAL-KF scheme can outperform the other two methods under different noise environments, e.g., the GAL-KF approach will result in 2.9 and 3.4 meters less of RMSE compared to the Beck-KF and TSLS-KF schemes, respectively, under $\sigma_n = 20$ meter in Fig. 9b, which is considered the major contribution of the proposed GAL-KF scheme.

**Example 9 (A General Case of GAL-KF Scheme under Realistic Environment).** In this example, the performance comparison is conducted for the GAL-KF scheme under the realistic environment. The same network layout setting as example 8 is adopted; while the noise setting is different by considering the NLOS in this example. In order to include the influence from the NLOS noise, the TOA model in (1) is rewritten as $r_i = \zeta_i + n_i + e_i$, where $e_i$ is denoted as the NLOS noise. Note that a range of NLOS mitigation algorithms [22], [23], [24] have been proposed in the literature to improve positioning accuracy. The standard deviation of the Gaussian noise is chosen as $\sigma_n = 10$. An exponential distribution $p_{e_i}(v)$ is assumed for the NLOS noise model of the TOA measurements as

$$p_{e_i}(v) = \begin{cases} \dfrac{1}{\lambda_i}\exp\left(-\dfrac{v}{\lambda_i}\right), & v > 0, \\ 0, & \text{otherwise}, \end{cases} \tag{51}$$

where $\lambda_i = c \cdot \tau_i = c \cdot \tau_m(\zeta_i)^{\varepsilon}\rho$. The parameter $\tau_i$ is the RMS delay spread between the $i$th BS and the MS. $\tau_m$ represents the median value of $\tau_i$, which is utilized as the $x$-axis in Figs. 10a and 10b. $\varepsilon$ is the path loss exponent which is assumed to be 0.5. The shadow fading factor $\rho$ is

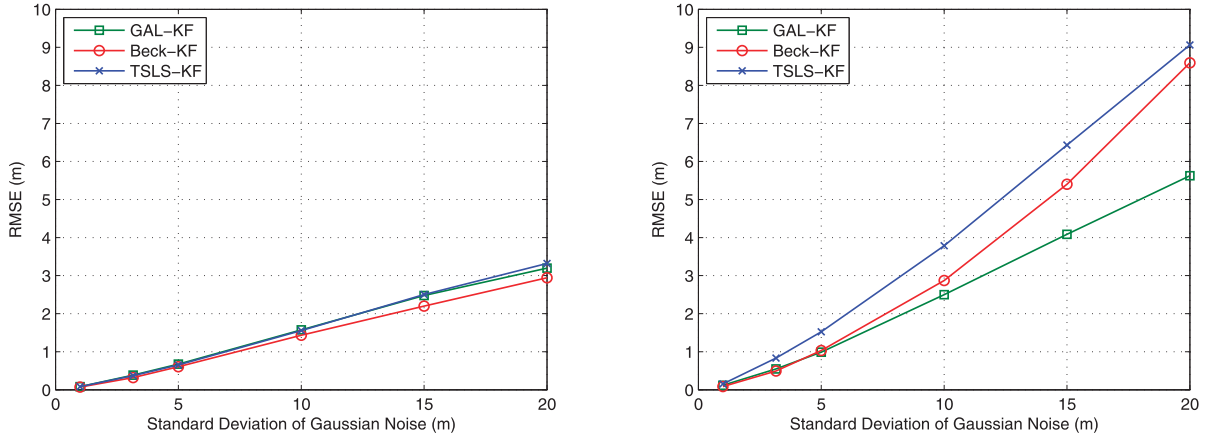


(a) MSs in the IPL. (b) MSs in the OPL.

Fig. 9. RMSE performance verus different standard deviations of Gaussian noise with network layout in Fig. 8.

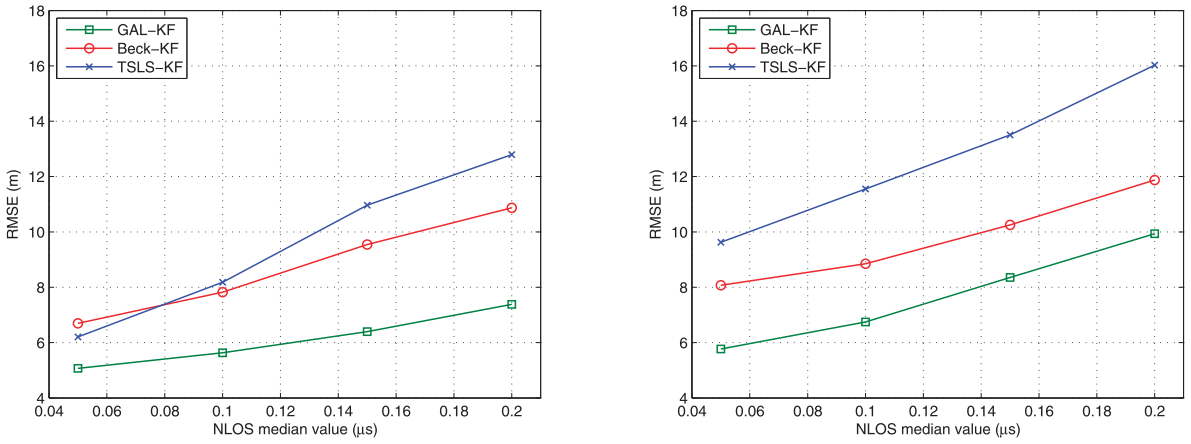


(a) MSs in the IPL. (b) MSs in the OPL.

Fig. 10. RMSE performance versus different NLOS median values with network layout in Fig. 8.

a log-normal random variable with zero mean and standard deviation $\sigma_\rho$ chosen as 4 dB in the simulations. Note that the median value $\tau_m = 0.1\ \mu s$ primarily fulfills the environment where the MS is located in the rural area [25].

Fig. 10a illustrates the performance comparison for the three schemes in the IPL under NLOS environment. It can be observed that the proposed GAL-KF approach can provide the smallest RMSE compared to the other two schemes, e.g., the GAL-KF scheme will result in 3.1 and 5.2 meters less of RMSE respectively under $\tau_m = 0.2\ \mu s$ compared to the Beck-KF and TSLS-KF methods. The reason is that the GAL-KF scheme is designed based on the minimization of L-CRLB by fictitiously adjusting the locations of BS. As mentioned in Section 2.3, the value of L-CRLB is affected by the distance between the BS and MS, which will be greatly influenced by the NLOS noises. Therefore, the effect from the NLOS noises has been implicitly considered in the design of GAL-KF scheme, which improves the location estimation performance. Moreover, Fig. 10b illustrates the performance comparison for the OPL scenario under NLOS environment. The proposed GAL-KF scheme can still outperform the other two methods, e.g., around 1.9 and 6 meters less of RMSE in comparison with the Beck-KF and TSLS-KF schemes under $\tau_m = 0.2\ \mu s$ in Fig. 9b. The merits of proposed GAL-KF scheme can therefore be observed.

## 6 Conclusion

The properties of linearized location estimation algorithms by introducing an additional variable are analyzed from the geometric point of view. By proposing the linearized location estimation problem-based CRLB (L-CRLB), the linearization loss from the linearized location estimation algorithms can be observed. In order to minimize the linearization loss, the geometry-assisted localization (GAL) algorithm is proposed in the paper by fictitiously moving the base stations in order to achieve the new geometric layout with minimum L-CRLB value. The GAL with two-step least squares implementation can enhance the estimation performance of the conventional two-step least squares estimator. By improving the initial estimation with the adoption of historical information, the GAL with Kalman filter scheme further outperforms the other location estimators with similar two-stage estimation structure.

## Acknowledgments

This work was in part funded by the Aiming for the Top University and Elite Research Center Development Plan, NSC 99-2628-E-009-005, the MediaTek research center at National Chiao Tung University, and the Telecommunication Laboratories at Chunghwa Telecom Co. Ltd, Taiwan.

## References

[1] A.H. Sayed, A. Tarighat, and N. Khajehnouri, "Network-Based Wireless Location: Challenges Faced in Developing Techniques for Accurate Wireless Location Information," *IEEE Signal Processing Magazine*, vol. 22, no. 4, pp. 25-40, July 2005.

[2] N. Patwari, J.N. Ash, S. Kyperountas, A.O. Hero III, R.L. Moses, and N.S. Correal, "Locating the Nodes: Cooperative Localization in Wireless Sensor Networks," *IEEE Signal Processing Magazine*, vol. 22, no. 4, pp. 54-69, July 2005.

[3] S. Gezici, Z. Tian, G.B. Giannakis, H. Kobayashi, A.F. Molisch, H.V. Poor, and Z. Sahinoglu, "Localization via Ultra-Wideband Radios: A Look at Positioning Aspects for Future Sensor Networks," *IEEE Signal Processing Magazine*, vol. 22, no. 4, pp. 70-84, July 2005.

[4] W.H. Foy, "Position-Location Solutions by Taylor-Series Estimation," *IEEE Trans. Aerospace Electronic Systems*, vol. 12, no. 2, pp. 187-194, Mar. 1976.

[5] J.J. Caffery Jr., "A New Approach to the Geometry of TOA Location," *Proc. IEEE Vehicular Technology Conf.*, pp. 1943-1949, Sept. 2000.

[6] N.B. Priyantha, "The Cricket Indoor Location System," PhD dissertation, Massachusetts Inst. of Technology, June 2005.

[7] K.W. Cheung, H.C. So, W.K. Ma, and Y.T. Chan, "Least Squares Algorithms for Time-of-Arrival-Based Mobile Location," *IEEE Trans. Signal Processing*, vol. 52, no. 4, pp. 1121-1128, Apr. 2004.

[8] X. Wang, Z. Wang, and B. O'Dea, "A TOA-Based Location Algorithm Reducing the Errors Due to Non-Line-of-Sight (NLOS) Propagation," *IEEE Trans. Vehicular Technology*, vol. 52, no. 1, pp. 112-116, Jan. 2003.

[9] Y.T. Chen and K.C. Ho, "A Simple and Efficient Estimator for Hyperbolic Location," *IEEE Trans. Signal Processing*, vol. 42, no. 8, pp. 1905-1915, Aug. 1994.

[10] K. Yu, "3-D Localization Error Analysis in Wireless Networks," *IEEE Trans. Wireless Comm.,* vol. 6, no. 10, pp. 3473-3481, Oct. 2007.
[11] P.-H. Tseng and K.-T. Feng, "Hybrid Network/Satellite-Based Location Estimation and Tracking Systems for Wireless Networks," *IEEE Trans. Vehicular Technology,* vol. 58, no. 9, pp. 5174-5189, Nov. 2009.
[12] J. Chaffee and J. Abel, "GDOP and the Cramer-Rao Bound," *Proc. IEEE Position Location and Navigation System Conf. (PLANS),* pp. 663-668, Apr. 1994.
[13] C. Chang and A. Sahai, "Estimation Bounds for Localization," *Proc. IEEE Conf. Sensor and Ad Hoc Comm. and Networks (SECON),* pp. 415-424, Oct. 2004.
[14] Y. Qi, H. Kobayashi, and H. Suda, "Analysis of Wireless Geolocation in a Non-Line-of-Sight Environment," *IEEE Trans. Wireless Comm.,* vol. 5, no. 3, pp. 672-681, Mar. 2006.
[15] I. Guvenc1, S. Gezici, and Z. Sahinoglu, "Fundamental Limits and Improved Algorithms for Linear Least-Squares Wireless Position Estimation," *Wireless Comm. and Mobile Computing,* vol. 12, pp. 1037-1052, Sept. 2010.
[16] P.-H. Tseng, C.-L. Chen, and K.-T. Feng, "An Unified Kalman Tracking Technique for Wireless Location Systems," *Proc. IEEE Int'l Symp. Wireless Pervasive Computing (ISWPC '07),* Feb. 2007.
[17] P.-H. Tseng, K.-T. Feng, Y.-C. Lin, and C.-L. Chen, "Wireless Location Tracking Algorithms for Environments with Insufficient Signal Sources," *IEEE Trans. Mobile Computing,* vol. 8, no. 12, pp. 1676-1689, Dec. 2009.
[18] L.-C. Chu, P.-H. Tseng, and K.-T. Feng, "GDOP-Assisted Location Estimation Algorithms in Wireless Location Systems," *Proc. IEEE GlobeCom,* pp. 1-5, Dec. 2008.
[19] S.M. Kay, *Fundamentals of Statistical Signal Processing: Estimation Theory.* Prentice Hall, 1993.
[20] A. Beck, P. Stoica, and L. Jian, "Exact and Approximate Solutions of Source Localization Problems," *IEEE Trans. Signal Processing,* vol. 56, no. 5, pp. 1770-1778, May 2008.
[21] K.W. Cheung, W.K. Ma, and H.C. So, "Accurate Approximation Algorithm for TOA-Based Maximum Likelihood Mobile Location Using Semidefinite Programming," *Proc. IEEE Int'l Conf. Acoustics, Speech, and Signal Processing (ICASSP '04),* vol. 2, pp. 145-148, May 2004.
[22] L. Cong and W. Zhuang, "Nonline-of-Sight Error Mitigation in Mobile Location," *IEEE Trans. Wireless Comm.,* vol. 4, no. 2, pp. 560-573, Mar. 2005.
[23] W. Kim, J. Lee, and G.-I. Jeep, "The Interior-Point Method for an Optimal Treatment of Bias in Trilateration Location," *IEEE Trans. Vehicular Technology,* vol. 55, no. 4, pp. 1291-1301, July 2006.
[24] H. Miao, K. Yu, and M. Juntti, "Positioning for NLOS Propagation: Algorithm Derivations and Cramér-Rao Bounds," *IEEE Trans. Vehicular Technology,* vol. 56, no. 5, pp. 2568-2580, Sept. 2007.
[25] L.J. Greenstein, V. Erceg, Y.S. Yeh, and M.V. Clark, "A New Path-Gain/Delay-Spread Propagation Model for Digital Cellular Channels," *IEEE Trans. Vehicular Technology,* vol. 46, no. 2, pp. 477-485, May 1997.

**Po-Hsuan Tseng** received the BS and PhD degrees in communication engineering from the National Chiao Tung University, Hsinchu, Taiwan, in 2005 and 2011, respectively. Since August 2012, he has been an assistant professor with the Department of Electronic Engineering, National Taipei University of Technology (NTUT), Taipei, Taiwan. From January 2010 to October 2010, he was a visiting researcher with the University of California at Davis. His research interests are in the areas of signal processing for networking and communications, including location estimation and tracking, cooperative localization, and mobile broadband wireless access system design. He is an honorary member of the Phi Tau Phi Scholastic Honor Society of R.O.C. He is a member of the IEEE.

**Kai-Ten Feng** received the BS degree from the National Taiwan University, Taipei, in 1992, the MS degree from the University of Michigan, Ann Arbor, in 1996, and the PhD degree from the University of California, Berkeley, in 2000. Between 2000 and 2003, he was an in-vehicle development manager/senior technologist with OnStar Corporation, a subsidiary of General Motors Corporation, where he worked on the design of future telematics platforms and in-vehicle networks. Since August 2011, he has been a full professor with the Department of Electrical and Computer Engineering, National Chiao Tung University (NCTU), Hsinchu, Taiwan, where he was an associate professor and assistant professor from August 2007 to July 2011 and from February 2003 to July 2007, respectively. From July 2009 to March 2010, he was a visiting scholar with the Department of Electrical and Computer Engineering, University of California at Davis. He has also been the Convener of the NCTU Leadership Development Program since August 2011. Since October 2011, he has served as the director of the Digital Content Production Center at the same university. His current research interests include broadband wireless networks, cooperative and cognitive networks, smart phone and embedded system designs, wireless location technologies, and intelligent transportation systems. He received the Best Paper Award from the Spring 2006 IEEE Vehicular Technology Conference, which ranked his paper first among the 615 accepted papers. He also received the Outstanding Youth Electrical Engineer Award in 2007 from the Chinese Institute of Electrical Engineering and the Distinguished Researcher Award from NCTU in 2008, 2010, and 2011, respectively. He has served on the technical program committees of the Vehicular Technology, International Communications, and Wireless Communications and Networking Conferences. He is a member of the IEEE and the IEEE Computer Society.